



L2A+

Ref: *Ref: ESA AO/1-11041/22/I-NS*

DI05: *Output Data Product (OP) - V2*

Page: 1

L2A+

Enhanced Aeolus L2A for depolarizing targets and impact on aerosol research and NWP

-

**Output Data Product
(OP)**

**Deliverable Item 05
[DI05]
(Version 2.0)**

Submitted to: Edward Malina (ESA)

	Name	Function	Date
Prepared by:	E. Proestakis	WP1000 – NOA	04/2024
	K. Rizos	WP3000 – NOA	04/2024
	A. Gkikas	WP3000 – NOA	04/2024
	A. A. Floutsi	WP2000 – TROPOS	04/2024
	H. Baars	WP2000 – TROPOS – CoPI	04/2024
Approved by:	V. Amiridis	PI	04/2024

-

*National Observatory of Athens (NOA)
Institute for Astronomy, Astrophysics, Space Applications & Remote Sensing (IAASARS)
Vas. Pavlou & I. Metaxa, 15236 Penteli, Greece
&
Leibniz Institute for Tropospheric Research (TROPOS), Leipzig, Germany
&
European Centre for Medium-Range Weather Forecasts
[ECMWF]
Reading, United Kingdom*



L2A+

Ref: *Ref: ESA AO/1-11041/22/I-NS*

DI05: Output Data Product (OP) - V2

Page: 2

[This page is intentionally left blank.]



L2A+

Table of Contents

- 1. ESA-L2A+ DI05 – Overview..... 4
- 2. Unique feature mask over Mindelo and PollyXT optical properties 5
 - 2.1. Unique feature mask over Mindelo. 5
 - 3.2. PollyXT optical properties..... 7
 - 2.3. Access Credential. 18
 - 2.4. Contact Person..... 18
- 3. The L2A+ Product..... 19
 - 3.1. Introduction. 19
 - 3.2. Filename Format..... 19
 - 3.3. Indicative Study-Case: The Aeolus-Cabo Verde overpass on the 10th of September 2021..... 19
 - 3.3.1. Description of the atmospheric scene. 19
 - 3.3.2. Aeolus Optical Products. 22
 - 3.3.3. L2A and L2A+ products. 23
 - 3.3.4. L2A+ - ESA-eVe validation..... 24
 - 3.3.5. L2A+ - ESA-PollyXT validation. 26
 - 3.4. The L2A+ products..... 28
 - 3.5. Access Credential. 49
 - 3.6. Contact Person..... 49
- Acronyms and Abbreviations 50
- List of Figures..... 50
- List of Tables..... 52



1. ESA-L2A+ DI05 – Overview.

This document consists the Deliverable Item 05 (DI05) – Optical Products “OPs” – Version 2.0 (V2.0) submitted to the European Space Agency (ESA) by the consortium of the project “Enhanced Aeolus L2A for depolarizing targets and impact on aerosol research and NWP” (L2A+). DI05– OPs report on the (1) filenames, (2) variables, (3) process, (4) access credentials, and (5) contact persons of L2A+ WP2000 – “ASKOS ground-based datasets in support of L2A+” and WP3000 – “Development of the L2A+ aerosol product” output product datasets (Figure 1).

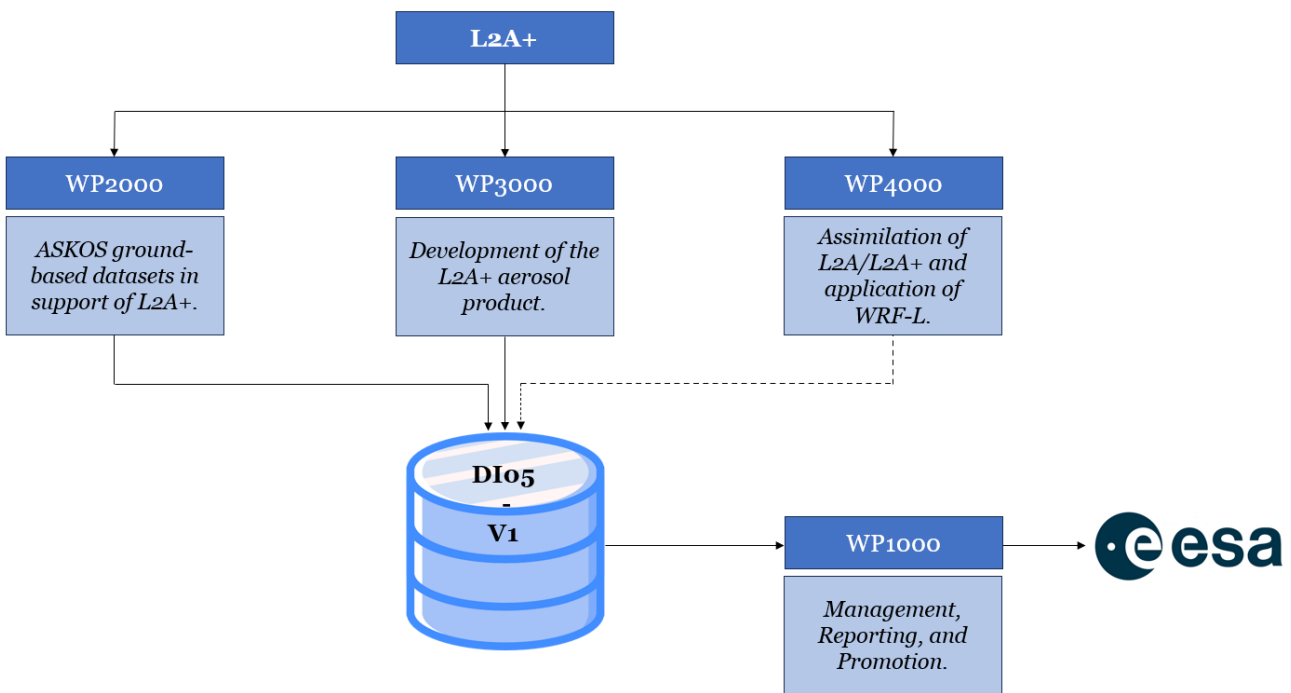


Figure 1: ESA-L2A+ WP2000, WP3000, and WP4000 input and outputs relevant to DI05.



2. Unique feature mask over Mindelo and PollyXT optical properties

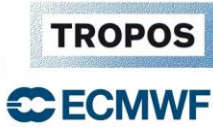
2.1. Unique feature mask over Mindelo.

The unique height-resolved feature mask utilizes lidar, cloud radar and microwave radiometer data and allows for high-performance cloud and feature detection (Combined Cloudnet + EARLINET lidar target categorization).

The filenames follow the structure: “YYYYMMDD_regridded_data_for_mindelo.nc”

Table 1: Provides the vertical profiles of the co-component of backscatter coefficient along the Aeolus overpass.

Group	Subgroup	Variable	Units	Dimensions	Description
FEATURE MASK	-	cloudnet_LWP	g/m ²	1D	Liquid water path
		cloudnet_radar_gas_attenuation	dB	2D	Two-way radar attenuation due to atmospheric gases
		cloudnet_radar_liquid_attenuation	dB	2D	Two-way radar attenuation due to liquid water
		cloudnet_radar_v	m/s	2D	Doppler velocity
		cloudnet_radar_width	m/s	2D	Spectral width
		cloudnet_radar_Z	dBZ	2D	Radar reflectivity factor
		cloudnet_radar_Z_error	dB	2D	Error in radar reflectivity factor
		cloudnet_target_classification	-	2D	Target classification
		combined_target_classification	-	2D	Target classification
		height	m	1D	Height above mean sea level
		model_pressure	Pa	2D	Pressure
		model_temperature	K	2D	Temperature
		polly_ang_532_1064	-	2D	Quasi backscatter-related Ångström exponent at 532-1064 nm
		polly_att_bsc_1064	sr ⁻¹ m ⁻¹	2D	Attenuated backscatter at 1064 nm



L2A+

	polly_att_bsc_532	sr ⁻¹ m ⁻¹	2D	Attenuated backscatter at 532 nm
	polly_bsc_1064	sr ⁻¹ m ⁻¹	2D	Quasi aerosol backscatter coefficients at 1064 nm
	polly_bsc_1064_quality_flag	-	2D	QC information
	polly_bsc_532	sr ⁻¹ m ⁻¹	2D	Quasi aerosol backscatter coefficients at 532 nm
	polly_bsc_532_quality_flag	-	2D	QC information
	polly_pardepol_532	-	2D	quasi particle depolarization ratio at 532 nm
	polly_target_classification	-	2D	Target classification
	polly_voldepol_532	-	2D	Volume depolarization ratio at 532 nm
	polly_voldepol_532_quality_flag	-	2D	QC information
	time	UTC	1D	Hours of day

Name	Long Name	Type
20210909_regridded_data_for_mindelo.nc	20210909_regridded_data_for_mindelo.nc	Local File
cloudnet_LWP	Liquid water path	1D
cloudnet_radar_gas_attenuation	Two-way radar attenuation due to atmospheric gases	2D
cloudnet_radar_liquid_attenuation	Two-way radar attenuation due to liquid water	2D
cloudnet_radar_v	Doppler velocity	2D
cloudnet_radar_width	Spectral width	2D
cloudnet_radar_Z	Radar reflectivity factor	2D
cloudnet_radar_Z_error	Error in radar reflectivity factor	2D
cloudnet_target_classification	Target classification	2D
combined_target_classification	Target classification	2D
height	Height Axis	1D
model_pressure	Pressure	2D
model_temperature	Temperature	2D
polly_ang_532_1064	quasi backscatter-related angstrom exponent at 532-1064	2D
polly_att_bsc_1064	attenuated backscatter at 1064 nm	2D
polly_att_bsc_532	attenuated backscatter at 532 nm	2D
polly_bsc_1064	quasi aerosol backscatter coefficients at 1064 nm	2D
polly_bsc_1064_quality_flag	polly bsc 1064 quality flag	2D
polly_bsc_532	quasi aerosol backscatter coefficients at 532 nm	2D
polly_bsc_532_quality_flag	polly bsc 532 quality flag	2D
polly_pardepol_532	quasi particle depolarization ratio at 532 nm	2D
polly_target_classification	Target classification	2D
polly_voldepol_532	volume depolarization ratio at 532 nm	2D
polly_voldepol_532_quality_flag	polly voldepol 532 quality flag	2D
time	Time Axis	1D

Figure 2: Indicative file output of Unique feature mask over Mindelo.



3.2. PollyXT optical properties.

The dataset includes vertically-resolved aerosol optical properties derived from the PollyXT ground-based, multiwavelength, Raman, polarization lidar measurements.

The filenames follow the structure:

“YYYY_MM_DD_weekday_CPV_HH_MM_SS_HHMM_HHMM_profiles.nc”

Table 2: Detailed description of the variables within the PollyXT profile product.

Group	Subgroup	Variable	Units	Dimension	Description
PollyXT PROFILE S	-	aerBsc_aeronet_1064	sr ⁻¹ m ⁻¹	1D	Aerosol backscatter coefficient at 1064 nm retrieved with constrained-AOD method
		aerBsc_aeronet_355	sr ⁻¹ m ⁻¹	1D	Aerosol backscatter coefficient at 355 nm retrieved with constrained-AOD method
		aerBsc_aeronet_532	sr ⁻¹ m ⁻¹	1D	Aerosol backscatter coefficient at 532 nm retrieved with constrained-AOD method
		aerBsc_klett_1064	sr ⁻¹ m ⁻¹	1D	Aerosol backscatter coefficient at 1064 nm retrieved with Klett method
		aerBsc_klett_355	sr ⁻¹ m ⁻¹	1D	Aerosol backscatter coefficient at 355 nm retrieved with Klett method
		aerBsc_klett_532	sr ⁻¹ m ⁻¹	1D	Aerosol backscatter coefficient at 532 nm retrieved with Klett method



	aerBsc_raman_1064	$\text{sr}^{-1} \text{ m}^{-1}$	1D	Aerosol backscatter coefficient at 1064 nm retrieved with Raman method
	aerBsc_raman_355	$\text{sr}^{-1} \text{ m}^{-1}$	1D	Aerosol backscatter coefficient at 355 nm retrieved with Raman method
	aerBsc_raman_532	$\text{sr}^{-1} \text{ m}^{-1}$	1D	Aerosol backscatter coefficient at 532 nm retrieved with Raman method
	aerBsc_RR_1064	$\text{sr}^{-1} \text{ m}^{-1}$	1D	Aerosol backscatter coefficient at 1064 nm retrieved with rotation Raman method
	aerBsc_RR_355	$\text{sr}^{-1} \text{ m}^{-1}$	1D	Aerosol backscatter coefficient at 355 nm retrieved with rotation Raman method
	aerBsc_RR_532	$\text{sr}^{-1} \text{ m}^{-1}$	1D	Aerosol backscatter coefficient at 532 nm retrieved with rotation Raman method
	aerExt_raman_1064	m^{-1}	1D	Aerosol extinction coefficient at 1064 nm retrieved with Raman method



	aerExt_raman_355	m ⁻¹	1D	Aerosol extinction coefficient at 355 nm retrieved with Raman method
	aerExt_raman_532	m ⁻¹	1D	Aerosol extinction coefficient at 532 nm retrieved with Raman method
	aerExt_RR_1064	m ⁻¹	1D	Aerosol extinction coefficient at 1064 nm retrieved with rotation Raman method
	aerExt_RR_355	m ⁻¹	1D	Aerosol extinction coefficient at 355 nm retrieved with rotation Raman method
	aerExt_RR_532	m ⁻¹	1D	Aerosol extinction coefficient at 532 nm retrieved with rotation Raman method
	aerLR_raman_1064	sr	1D	Aerosol lidar ratio at 1064 nm retrieved with Raman method
	aerLR_raman_355	sr	1D	Aerosol lidar ratio at 355 nm retrieved with Raman method
	aerLR_raman_532	sr	1D	Aerosol lidar ratio at 532 nm retrieved with Raman method



	aerLR_RR_1064	sr	1D	Aerosol lidar ratio at 1064 nm retrieved with rotation Raman method
	aerLR_RR_355	sr	1D	Aerosol lidar ratio at 355 nm retrieved with rotation Raman method
	aerLR_RR_532	sr	1D	Aerosol lidar ratio at 532 nm retrieved with rotation Raman method
	altitude	m	-	Height of lidar above mean sea level
	end_time	seconds since 1970-01-01 00:00:00 UTC	-	Time UTC of the end of the current measurement
	height	m	1D	Height above ground
	latitude	degrees north	-	Latitude of the site
	longitude	degrees east	-	Longitude of the site
	LR_aeronet_1064	sr	-	Aerosol lidar ratio at 1064 nm retrieved with constrained-AOD method
	LR_aeronet_355	sr	-	Aerosol lidar ratio at 355 nm retrieved with constrained-AOD method
	LR_aeronet_532	sr	-	Aerosol lidar ratio at 532 nm retrieved with constrained-AOD method



		parDepol_klett_1064	-	1D	Particle linear depolarization ratio at 1064 nm with Klett backscatter
		parDepol_klett_355	-	1D	Particle linear depolarization ratio at 355 nm with Klett backscatter
		parDepol_klett_532	-	1D	Particle linear depolarization ratio at 532 nm with Klett backscatter
		parDepol_raman_1064	-	1D	Particle linear depolarization ratio at 1064 nm with Raman backscatter
		parDepol_raman_355	-	1D	Particle linear depolarization ratio at 355 nm with Raman backscatter
		parDepol_raman_532	-	1D	Particle linear depolarization ratio at 532 nm with Raman backscatter
		pressure	hPa	1D	Air pressure
		reference_height_1064	m	1D	Reference height for 1064 nm
		reference_height_355	m	1D	Reference height for 355 nm
		reference_height_532	m	1D	Reference height for 532 nm
		RH	%	1D	Relative humidity
		shots	-	-	Accumulated laser shots
		start_time	seconds since 1970-01-01 00:00:	-	Time UTC of the start of the current measurement



			00 UTC		
		temperature	degree Celsius	1D	Air temperature
		uncertainty_aerBsc_aeronet_1064	sr ⁻¹ m ⁻¹	1D	Uncertainty of aerosol backscatter coefficient at 1064 nm
		uncertainty_aerBsc_aeronet_355	sr ⁻¹ m ⁻¹	1D	Uncertainty of aerosol backscatter coefficient at 355 nm
		uncertainty_aerBsc_aeronet_532	sr ⁻¹ m ⁻¹	1D	Uncertainty of aerosol backscatter coefficient at 532 nm
		uncertainty_aerBsc_klett_1064	sr ⁻¹ m ⁻¹	1D	Uncertainty of aerosol backscatter coefficient at 1064 nm
		uncertainty_aerBsc_klett_355	sr ⁻¹ m ⁻¹	1D	Uncertainty of aerosol backscatter coefficient at 355 nm
		uncertainty_aerBsc_klett_532	sr ⁻¹ m ⁻¹	1D	Uncertainty of aerosol backscatter coefficient at 532 nm
		uncertainty_aerBsc_raman_1064	sr ⁻¹ m ⁻¹	1D	Uncertainty of aerosol backscatter coefficient at 1064 nm
		uncertainty_aerBsc_raman_355	sr ⁻¹ m ⁻¹	1D	Uncertainty of aerosol backscatter coefficient at 355 nm
		uncertainty_aerBsc_raman_532	sr ⁻¹ m ⁻¹	1D	Uncertainty of aerosol backscatter coefficient at 532 nm
		uncertainty_aerBsc_RR_1064	sr ⁻¹ m ⁻¹	1D	Uncertainty of aerosol backscatter



					coefficient at 1064 nm
		uncertainty_aerBsc_RR_355	$\text{sr}^{-1} \text{ m}^{-1}$	1D	Uncertainty of aerosol backscatter coefficient at 355 nm
		uncertainty_aerBsc_RR_532	$\text{sr}^{-1} \text{ m}^{-1}$	1D	Uncertainty of aerosol backscatter coefficient at 532 nm
		uncertainty_aerExt_raman_1064	m^{-1}	1D	Uncertainty of aerosol extinction coefficient at 1064 nm
		uncertainty_aerExt_raman_355	m^{-1}	1D	Uncertainty of aerosol extinction coefficient at 355 nm
		uncertainty_aerExt_raman_532	m^{-1}	1D	Uncertainty of aerosol extinction coefficient at 532 nm
		uncertainty_aerExt_RR_1064	m^{-1}	1D	Uncertainty of aerosol extinction coefficient at 1064 nm
		uncertainty_aerExt_RR_355	m^{-1}	1D	Uncertainty of aerosol extinction coefficient at 355 nm
		uncertainty_aerExt_RR_532	m^{-1}	1D	Uncertainty of aerosol extinction coefficient at 532 nm
		uncertainty_aerLR_raman_1064	m^{-1}	1D	Uncertainty of aerosol lidar ratio at 1064 nm
		uncertainty_aerLR_raman_355	sr	1D	Uncertainty of aerosol lidar ratio at 355 nm
		uncertainty_aerLR_raman_532	sr	1D	Uncertainty of aerosol lidar



				ratio at 532 nm	
		uncertainty_aerLR_RR_1064	sr	1D	Uncertainty of aerosol lidar ratio at 1064 nm
		uncertainty_aerLR_RR_355	sr	1D	Uncertainty of aerosol lidar ratio at 355 nm
		uncertainty_aerLR_RR_532	sr	1D	Uncertainty of aerosol lidar ratio at 532 nm
		uncertainty_parDepol_klett_1064	-	1D	Uncertainty of particle linear depolarization ratio at 1064 nm with Klett backscatter
		uncertainty_parDepol_klett_355	-	1D	Uncertainty of particle linear depolarization ratio at 355 nm with Klett backscatter
		uncertainty_parDepol_klett_532	-	1D	Uncertainty of particle linear depolarization ratio at 532 nm with Klett backscatter
		uncertainty_parDepol_raman_1064	-	1D	Uncertainty of particle linear depolarization ratio at 1064 nm with Raman backscatter
		uncertainty_parDepol_raman_355	-	1D	Uncertainty of particle linear depolarization ratio at 355 nm with Raman backscatter
		uncertainty_parDepol_raman_532	-	1D	Uncertainty of particle linear depolarization ratio at 532 nm with Raman backscatter



		uncertainty_volDepol_klett_1064	-	1D	Uncertainty of volume depolarization ratio at 1064 nm
		uncertainty_volDepol_klett_355	-	1D	Uncertainty of volume depolarization ratio at 355 nm
		uncertainty_volDepol_klett_532	-	1D	Uncertainty of volume depolarization ratio at 532 nm
		uncertainty_volDepol_raman_1064	-	1D	Uncertainty of volume depolarization ratio at 1064 nm
		uncertainty_volDepol_raman_355	-	1D	Uncertainty of volume depolarization ratio at 355 nm
		uncertainty_volDepol_raman_532	-	1D	Uncertainty of volume depolarization ratio at 532 nm
		uncertainty_WVMR	g/km	1D	Absolute water vapor mixing ratio uncertainty
		volDepol_klett_1064	-	1D	Volume linear depolarization ratio at 1064 nm with the same smoothing as Klett method
		volDepol_klett_355	-	1D	Volume linear depolarization ratio at 355 nm with the same smoothing as Klett method
		volDepol_klett_532	-	1D	Volume linear depolarization ratio at 532 nm with the same



					smoothing as Klett method
		volDepol_raman_1064	-	1D	Volume linear depolarization ratio at 1064 nm with the same smoothing as Raman method
		volDepol_raman_355	-	1D	Volume linear depolarization ratio at 355 nm with the same smoothing as Raman method
		volDepol_raman_532	-	1D	Volume linear depolarization ratio at 532 nm with the same smoothing as Raman method
		WVMR	g/kg	1D	Water vapor mixing ratio
		WVMR_no_QC	g/kg	1D	Water vapor mixing ratio without quality control
		WVMR_rel_err	-	1D	Relative error of the water vapor mixing ratio
		zenith_angle	degree	-	Zenith angle



L2A+

Ref: Ref: ESA AO/1-11041/22/I-NS

DI05: Output Data Product (OP) - V2

Page: 17

Name	Long Name	Type
2021_09_01_Wed_CPV_00_01_01_0001_0100_profiles.nc	2021_09_01_Wed_CPV_00_01_01_0001_0100_profiles.nc	Local File
aerBsc_aeronet_1064	aerosol backscatter coefficient at 1064 nm retrieved with constrained-...	1D
aerBsc_aeronet_355	aerosol backscatter coefficient at 355 nm retrieved with constrained-A...	1D
aerBsc_aeronet_532	aerosol backscatter coefficient at 532 nm retrieved with constrained-A...	1D
aerBsc_klett_1064	aerosol backscatter coefficient at 1064 nm retrieved with Klett method	1D
aerBsc_klett_355	aerosol backscatter coefficient at 355 nm retrieved with Klett method	1D
aerBsc_klett_532	aerosol backscatter coefficient at 532 nm retrieved with Klett method	1D
aerBsc_raman_1064	aerosol backscatter coefficient at 1064 nm retrieved with Raman method	1D
aerBsc_raman_355	aerosol backscatter coefficient at 355 nm retrieved with Raman method	1D
aerBsc_raman_532	aerosol backscatter coefficient at 532 nm retrieved with Raman method	1D
aerBsc_RR_1064	aerosol backscatter coefficient at 1064 nm retrieved with rotation Ram...	1D
aerBsc_RR_355	aerosol backscatter coefficient at 355 nm retrieved with rotation Rama...	1D
aerBsc_RR_532	aerosol backscatter coefficient at 532 nm retrieved with rotation Rama...	1D
aerExt_raman_1064	aerosol extinction coefficient at 1064 nm retrieved with Raman method	1D
aerExt_raman_355	aerosol extinction coefficient at 355 nm retrieved with Raman method	1D
aerExt_raman_532	aerosol extinction coefficient at 532 nm retrieved with Raman method	1D
aerExt_RR_1064	aerosol extinction coefficient at 1064 nm retrieved with rotation Rama...	1D
aerExt_RR_355	aerosol extinction coefficient at 355 nm retrieved with rotation Raman ...	1D
aerExt_RR_532	aerosol extinction coefficient at 532 nm retrieved with rotation Raman ...	1D
aerLR_raman_1064	aerosol lidar ratio at 1064 nm retrieved with Raman method	1D
aerLR_raman_355	aerosol lidar ratio at 355 nm retrieved with Raman method	1D
aerLR_raman_532	aerosol lidar ratio at 532 nm retrieved with Raman method	1D
aerLR_RR_1064	aerosol lidar ratio at 1064 nm retrieved with rotation Raman method	1D
aerLR_RR_355	aerosol lidar ratio at 355 nm retrieved with rotation Raman method	1D
aerLR_RR_532	aerosol lidar ratio at 532 nm retrieved with rotation Raman method	1D
altitude	Height of lidar above mean sea level	—
end_time	Time UTC to finish the current measurement	—
height	Height above the ground	1D
latitude	Latitude of the site	—
longitude	Longitude of the site	—
LR_aeronet_1064	aerosol lidar ratio at 1064 nm retrieved with constrained-AOD method	—
LR_aeronet_355	aerosol lidar ratio at 355 nm retrieved with constrained-AOD method	—
LR_aeronet_532	aerosol lidar ratio at 532 nm retrieved with constrained-AOD method	—
parDepol_klett_1064	particle linear depolarization ratio at 1064 nm with Klett backscatter	1D
parDepol_klett_355	particle linear depolarization ratio at 355 nm with Klett backscatter	1D
parDepol_klett_532	particle linear depolarization ratio at 532 nm with Klett backscatter	1D
parDepol_raman_1064	particle linear depolarization ratio at 1064 nm with Raman backscatter	1D
parDepol_raman_355	particle linear depolarization ratio at 355 nm with Raman backscatter	1D
parDepol_raman_532	particle linear depolarization ratio at 532 nm with Raman backscatter	1D
pressure	pressure	1D
reference_height_1064	reference height for 1064 nm	1D
reference_height_355	reference height for 355 nm	1D
reference_height_532	reference height for 532 nm	1D
RH	relative humidity	1D
shots	accumulated laser shots	—
start_time	Time UTC to start the current measurement	—
temperature	temperature	1D
uncertainty_aerBsc_aeronet_1064	uncertainty of aerosol backscatter coefficient at 1064 nm	1D
uncertainty_aerBsc_aeronet_355	uncertainty of aerosol backscatter coefficient at 355 nm	1D
uncertainty_aerBsc_aeronet_532	uncertainty of aerosol backscatter coefficient at 532 nm	1D
uncertainty_aerBsc_klett_1064	uncertainty of aerosol backscatter coefficient at 1064 nm	1D
uncertainty_aerBsc_klett_355	uncertainty of aerosol backscatter coefficient at 355 nm	1D
uncertainty_aerBsc_klett_532	uncertainty of aerosol backscatter coefficient at 532 nm	1D
uncertainty_aerBsc_raman_1064	uncertainty of aerosol backscatter coefficient at 1064 nm	1D
uncertainty_aerBsc_raman_355	uncertainty of aerosol backscatter coefficient at 355 nm	1D
uncertainty_aerBsc_raman_532	uncertainty of aerosol backscatter coefficient at 532 nm	1D
uncertainty_aerBsc_RR_1064	uncertainty of aerosol backscatter coefficient at 1064 nm	1D
uncertainty_aerBsc_RR_355	uncertainty of aerosol backscatter coefficient at 355 nm	1D
uncertainty_aerBsc_RR_532	uncertainty of aerosol backscatter coefficient at 532 nm	1D
uncertainty_aerExt_raman_1064	uncertainty of aerosol extinction coefficient at 1064 nm	1D



L2A+

uncertainty_aerExt_raman_355	uncertainty of aerosol extinction coefficient at 355 nm	1D
uncertainty_aerExt_raman_532	uncertainty of aerosol extinction coefficient at 532 nm	1D
uncertainty_aerExt_RR_1064	uncertainty of aerosol extinction coefficient at 1064 nm	1D
uncertainty_aerExt_RR_355	uncertainty of aerosol extinction coefficient at 355 nm	1D
uncertainty_aerExt_RR_532	uncertainty of aerosol extinction coefficient at 532 nm	1D
uncertainty_aerLR_raman_1064	uncertainty of aerosol lidar ratio at 1064 nm	1D
uncertainty_aerLR_raman_355	uncertainty of aerosol lidar ratio at 355 nm	1D
uncertainty_aerLR_raman_532	uncertainty of aerosol lidar ratio at 532 nm	1D
uncertainty_aerLR_RR_1064	uncertainty of aerosol lidar ratio at 1064 nm	1D
uncertainty_aerLR_RR_355	uncertainty of aerosol lidar ratio at 355 nm	1D
uncertainty_aerLR_RR_532	uncertainty of aerosol lidar ratio at 532 nm	1D
uncertainty_parDepol_klett_1064	uncertainty of particle linear depolarization ratio at 1064 nm with Klett ...	1D
uncertainty_parDepol_klett_355	uncertainty of particle linear depolarization ratio at 355 nm with Klett b...	1D
uncertainty_parDepol_klett_532	uncertainty of particle linear depolarization ratio at 532 nm with Klett b...	1D
uncertainty_parDepol_raman_1064	uncertainty of particle linear depolarization ratio at 1064 nm with Rama...	1D
uncertainty_parDepol_raman_355	uncertainty of particle linear depolarization ratio at 355 nm with Raman...	1D
uncertainty_parDepol_raman_532	uncertainty of particle linear depolarization ratio at 532 nm with Raman...	1D
uncertainty_volDepol_klett_1064	uncertainty of volume depolarization ratio at 1064 nm	1D
uncertainty_volDepol_klett_355	uncertainty of volume depolarization ratio at 355 nm	1D
uncertainty_volDepol_klett_532	uncertainty of volume depolarization ratio at 532 nm	1D
uncertainty_volDepol_raman_1064	uncertainty of volume depolarization ratio at 1064 nm	1D
uncertainty_volDepol_raman_355	uncertainty of volume depolarization ratio at 355 nm	1D
uncertainty_volDepol_raman_532	uncertainty of volume depolarization ratio at 532 nm	1D
uncertainty_WVMR	absolute water vapor mixing ratio uncertainty	1D
volDepol_klett_1064	volume linear depolarization ratio at 1064 nm with the same smoothing ...	1D
volDepol_klett_355	volume linear depolarization ratio at 355 nm with the same smoothing a...	1D
volDepol_klett_532	volume linear depolarization ratio at 532 nm with the same smoothing a...	1D
volDepol_raman_1064	volume linear depolarization ratio at 1064 nm with the same smoothing ...	1D
volDepol_raman_355	volume linear depolarization ratio at 355 nm with the same smoothing a...	1D
volDepol_raman_532	volume linear depolarization ratio at 532 nm with the same smoothing a...	1D
WVMR	water vapor mixing ratio	1D
WVMR_no_QC	water vapor mixing ratio without Quality control	1D
WVMR_rel_error	relative error of the water vapor mixing ratio	1D
zenith_angle	laser pointing angle with respect to the zenith	—

Figure 3: Indicative file output of PollyXT optical properties.

2.3. Access Credential.

Access to the ESA-L2A+ products are provided according to the following access credentials:

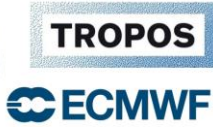
Table 3: ESA L2A+ WP2000 access credentials.

WP2000	
Protocol:	SFTP (Port 22)
Username:	l2aplus_wp2000
Password:	eYst5kuxngzn
Host:	react.space.noa.gr

2.4. Contact Person.

Contact:

Users can contact with Athina Floutsi (floutsi@tropos.de) or/and Holger Baars (baars@tropos.de) for any further details and clarifications regarding the L2A+ dataset outputs of L2A+ WP2000.



3. The L2A+ Product.

3.1. Introduction.

This section provides an overview of the L2A+ aerosol product established on the basis of Aeolus. More specifically, the product is derived on the basis of a synergistic approach involving spaceborne retrievals from multi-sensors in conjunction with reanalysis numerical outputs and reference ground-based measurements. The period of interest includes the months of September of 2021 and June, September of 2022 which coincides with the Joint Aeolus Tropical Atlantic Campaign (JATAC), on the islands of Cabo Verde during the ASKOS experiment. Information on the development is provided in the framework of the ESA L2A+ DI03 entitled “Description of the Algorithm Developments (ALGO)”. The present section provides an overview of the L2A+ products in terms of filename format (Sect.3.2), the L2A+ output products for an indicative Aeolus study case (Sect.3.3), the basic products included in the output Netcdf file (Sect.3.4), access credentials (Sect.3.5), and contact person information (Sect.3.6)

3.2. Filename Format.

L2A+ filename: “AE_OPER_ALD_U_N_2A_DD MMM_YYYY_hh_mm_ss_hh_mm_ss.nc”

Table 4: L2A+ filename descriptor.

Filename Descriptor		Explanation
AE	⇒	Aeolus mission
OPER	⇒	File class: Routine operations
ALD	⇒	Data product from the Aladin instrument
U	⇒	Unconsolidated
N	⇒	Nominal instrument operation
2A	⇒	Product ID: Level 2A product
yyyymmddThmmsszzz	⇒	start time of sensing (date/time string: precision 1 ms)
‘uuuuuuuuu’	⇒	duration/sensing period
‘oooooo’	⇒	start absolute orbit number
‘vvvv’	⇒	file version number

3.3. Indicative Study-Case: The Aeolus-Cabo Verde overpass on the 10th of September 2021.

3.3.1. Description of the atmospheric scene.

Figure 4a illustrates the L2A+ region of interest with the blue-colored line indicating the ascending ALADIN’s measurement track for the given case. Next, Figure 4b illustrates for the specific study case, the time-closest binary cloud mask (CMA) product retrieved from the SEVIRI CLAAS-3 cloud dataset which as we can see in the figure, describes the scene type (either 'clear' or 'cloudy') on a pixel level. The Aeolus’s ascending orbit is also depicted on the same figure with the red-coloured line. Based on the specific cloud-filtering procedure, the Aeolus SCA, SCA mid-bin and MLE backscatter retrievals, throughout the probed atmosphere by ALADIN, have been excluded from the analysis when the cloud fraction in each BRC profile exceeds a given threshold value (60% in this case).



Aeolus Orbit

MSG Cloud Coverage

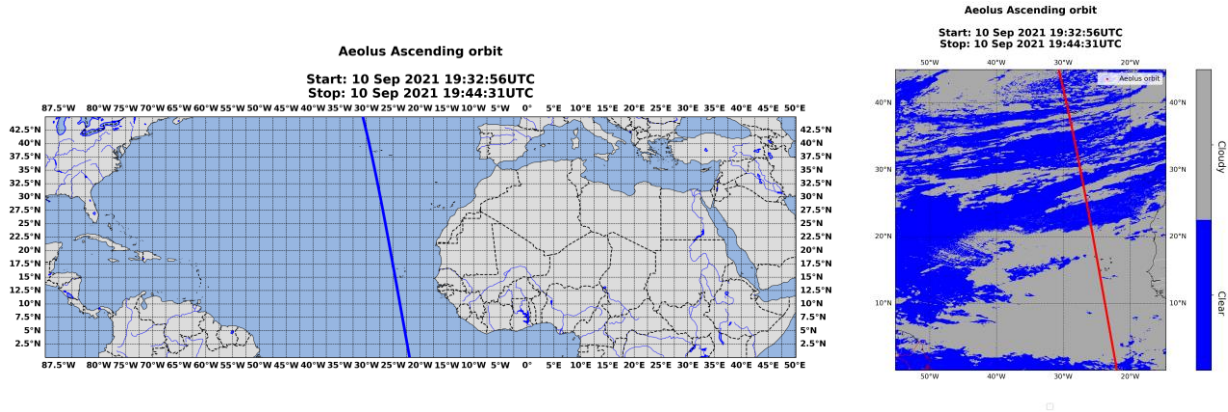
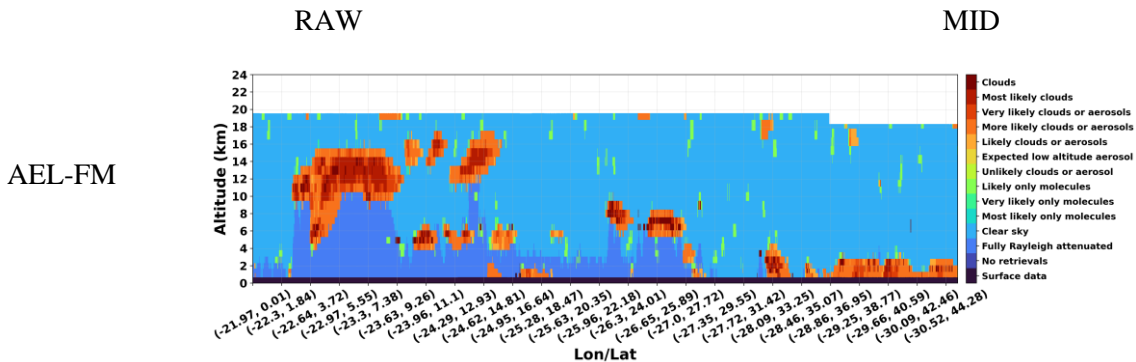


Figure 4: a) Aeolus ascending orbit (id: 017679) over the L2A+ RoI on 10th September 2021 and b) the time-closest spatial distribution of clouds derived from the binary cloud-mask product of MSG-SEVIRI CLAAS-3 dataset.

In Figure 5a, the retrieved AEL-FM feature-mask product along the given Aeolus’s measurement track is presented where we can observe the classified features of the probed atmospheric scene. It can be seen that the features associated with “strong” returns mainly attributed to clouds or high optically thick aerosol layers are colorized in brown and orange respectively while those associated with the molecular atmosphere or clear sky conditions are colorized in green and cyan respectively. According to the figure, one can clearly distinguish a large number of strong features that have been classified as (likely and most likely) clouds (FM values of 6 to 10) along the largest part of the given Aeolus’s measurement track and especially between latitudes of 0 and 7° N and altitudes between 4 and 14 km above the ground. Following our filtering methodology, these features can be detected and excluded from the analysis in order to acquire the pure aerosol profiles. In the two figures below, the transformed feature mask product to the Aeolus’s horizontal and vertical resolution is provided separately for the regular Aeolus’s vertical scale (24 vertical bins) (Figure 5b) and middle-bin (23 vertical bins) scale (Figure 5c) with each bin expressing the cloud fraction (in %) of the specific BRC bin after computing the total percentage of cloud-contaminated measurements for the specific bin. Based on the transformed feature mask product, all Aeolus’s BRC bins with cloud fraction exceeding 0% were excluded from the analysis with the corresponding bins of the SCA, SCA mid-bin and MLE backscatter profiles.



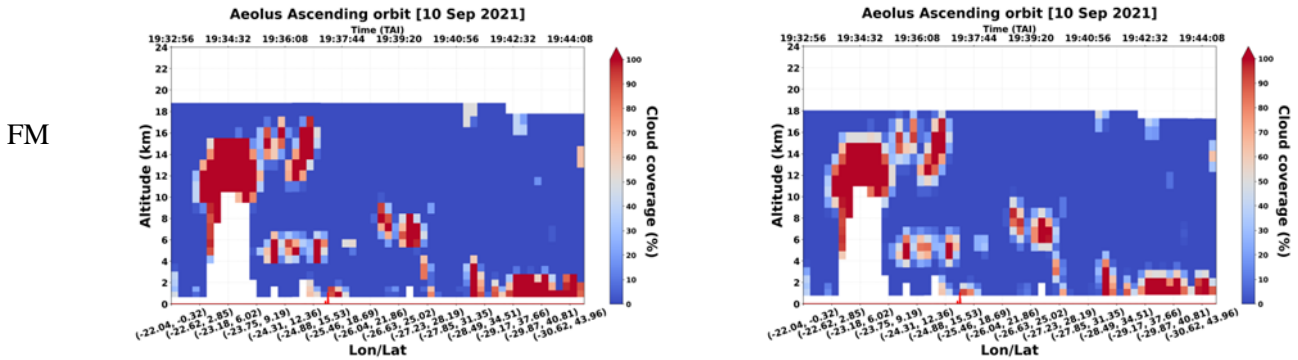


Figure 5: a) AEL-FM feature mask product along the Aeolus orbit (id: 017679) on 10th September 2021 and the transformed feature mask product on the Aeolus vertical and horizontal resolution for the b) regular (24 bins) and c) middle-bin scale (23 bins).

In the figure below, we present the horizontally integrated and vertically resolved Aeolus-like dust mass concentration profiles from CAMS along the Aeolus orbit (id: 017679), provided separately for the regular (Figure 6a) and middle-bin (Figure 6c) Aeolus' vertical scales (24, and 23 vertical bins respectively). According to the figure, a dust layer is identified over the latitudinal band of 5°- 25°N and up to 6km with elevated dust mass concentration values exceeding in many cases the value of 50 $\mu\text{g}/\text{m}^3$. Additionally, for both vertical scales, the vertical profiles of the dust-to-total mass concentration ratio values (in percentage) along the Aeolus measurement track are also depicted in Figures 6b, and d. Based on both parameters retrieved from CAMS, the pure dust profiles were derived after eliminating all the BRC bins with dust concentration below 1.3 $\mu\text{g}/\text{m}^3$ (median value) and dust-to-total ratio below 50%.

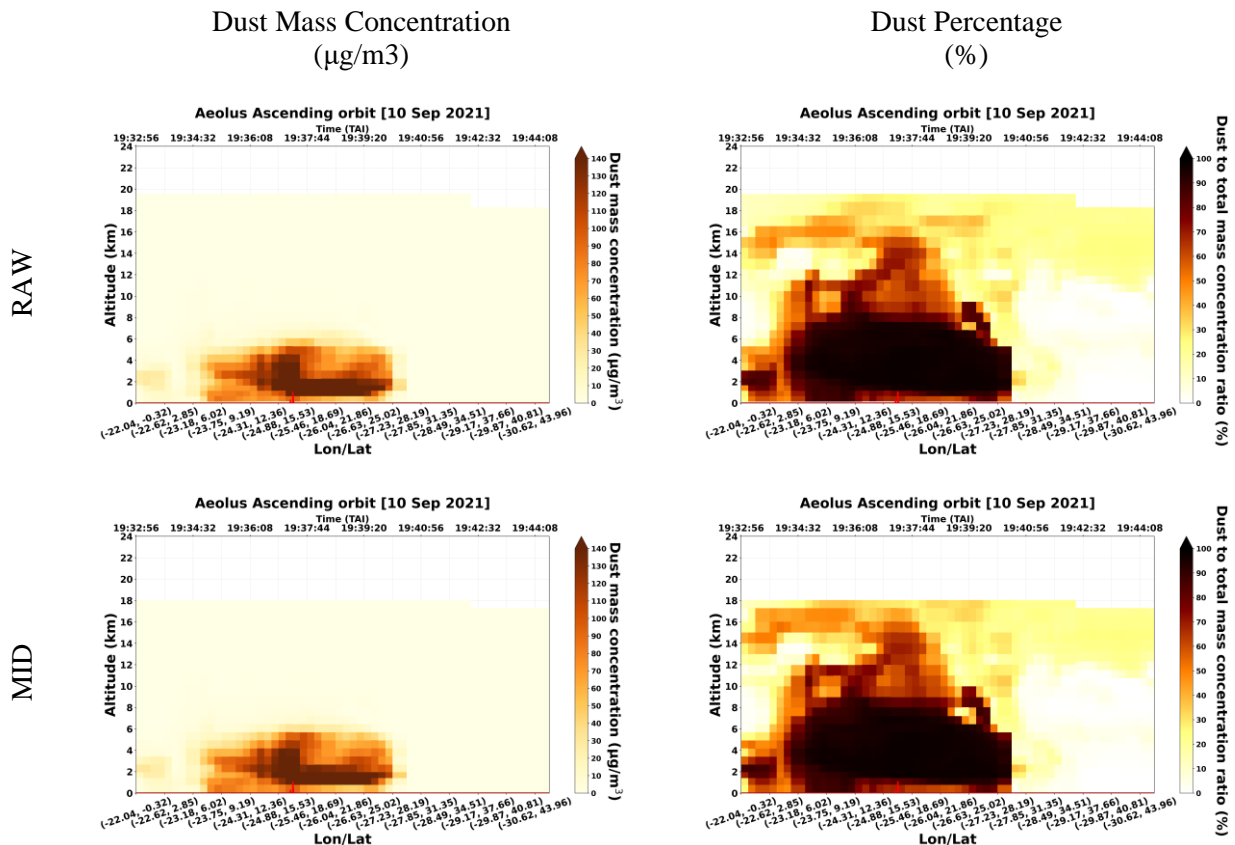


Figure 6: Vertical profiles of CAMS dust mass concentration and dust-to-total aerosol mass concentration ratio along the Aeolus orbit (id: 017679) provided in the regular (a, b) and middle-bin (c, d) vertical scales on the 10th of September 2021.

For the specific study case, the time-closest vertical profiles of CALIPSO total backscatter coefficient at 532 nm (Figure 7a), particulate depolarization ratio at 532 nm (Figure 7b) and the quality-assured (QA) pure-aerosol (Figure 7c) and pure-dust backscatter coefficient (Figure 7d) are also illustrated.

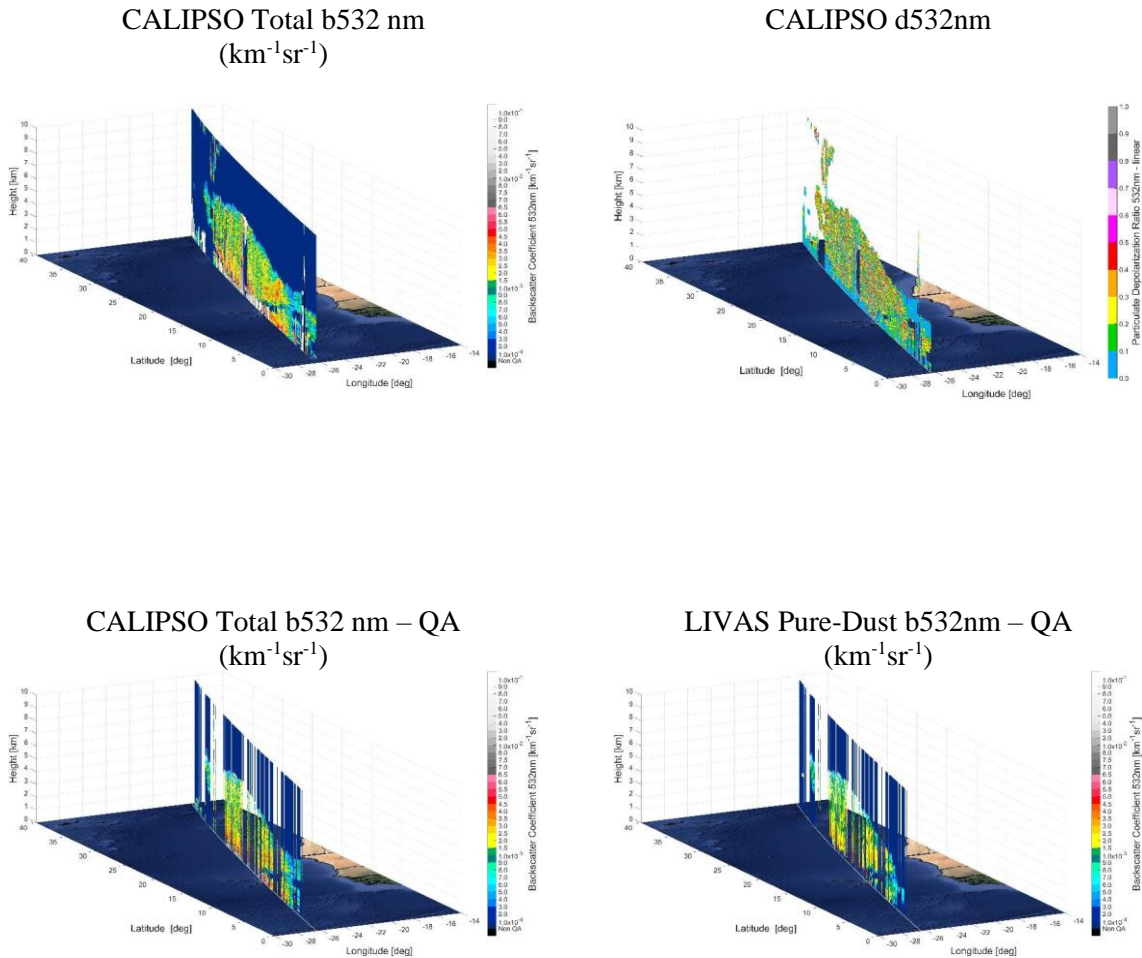


Figure 7: (a) CALIPSO total backscatter coefficient at 532 nm. (b) CALIPSO particulate depolarization ratio at 532 nm (c) CALIPSO QA pure-aerosol total backscatter coefficient at 532 nm (d) CALIPSO QA pure-dust backscatter coefficient at 532 nm.

3.3.2. Aeolus Optical Products.

In figure 8, the left panel illustrates the vertical profiles of the raw (unprocessed) Aeolus L2A retrievals of backscatter coefficient at 355 nm along the Aeolus overpass (id 017679), produced by the SCA, SCA mid-bin and MLE algorithms, while the right panel depicts the quality-assured (QA) backscatter profiles derived from the corresponding algorithms after implementing the cloud-filtering methodology using both the AEL-FM feature mask and MSG-SEVIRI Claas-3 cloud-mask retrievals. It has to be noted that the later ones correspond to the pure-aerosol backscatter profiles along the Aeolus overpass, since most of bins were rejected from the cloud-filtering process.

Aeolus b355nm - Raw

Aeolus b355nm – AEL-FM & MSG QA

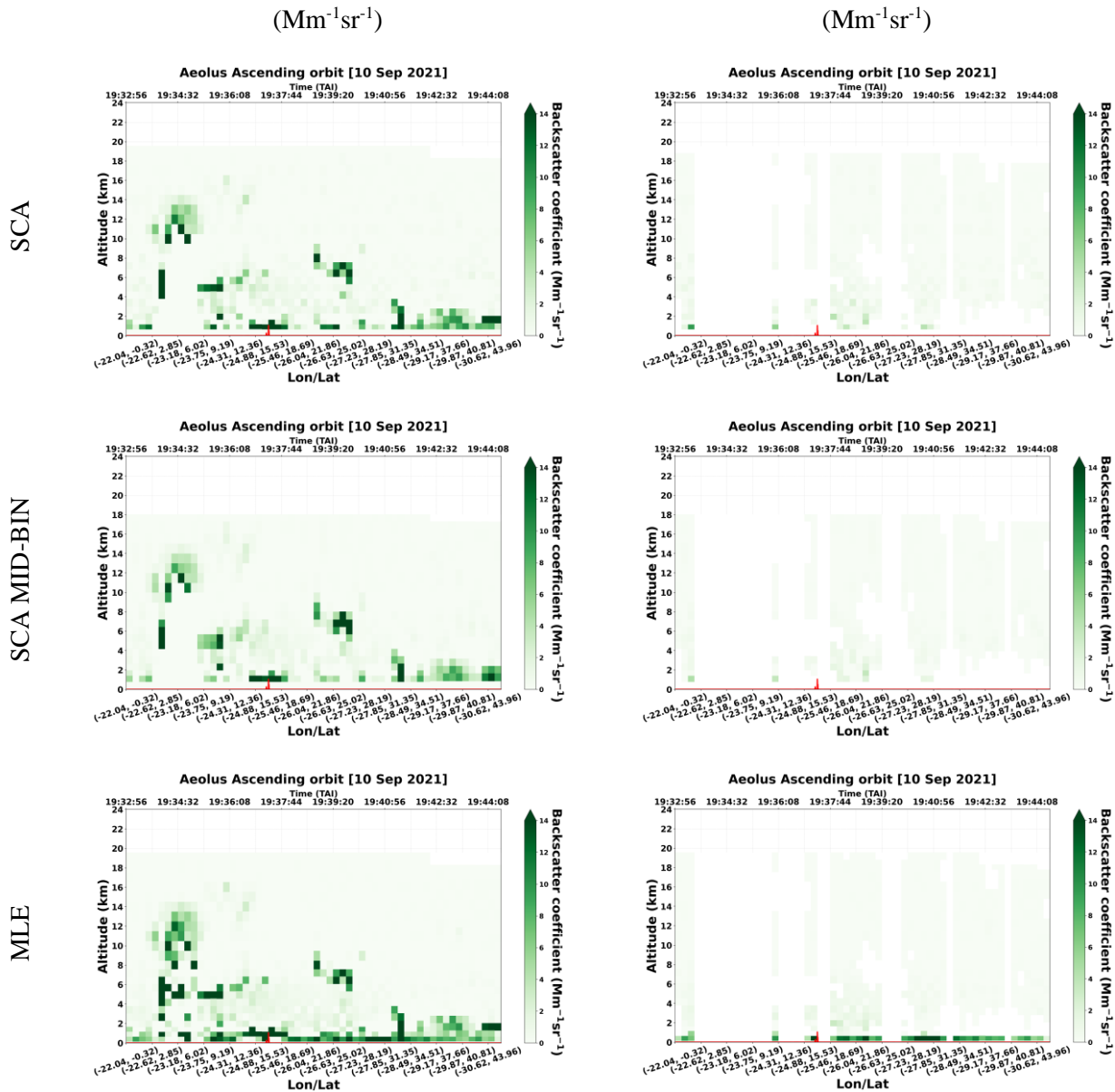


Figure 8: Raw Aeolus L2A backscatter profiles at 355 nm along the Aeolus orbit (id 017679) retrieved from the SCA, SCA mid-bin and MLE algorithms (left panel) and the corresponding QA pure-aerosol backscatter profiles at 355 nm for the SCA, SCA mid-bin and MLE algorithms (right panel).

3.3.3. L2A and L2A+ products.

Figure 9 gives for the given study case, an example of the pure-dust Aeolus co-polar backscatter profiles at 355 nm produced with the SCA and SCA mid-bin algorithms and the associated missing cross-polar backscatter component for each profile. Using both backscatter components (co + cross) the total (L2A+) backscatter profiles at 355 nm were derived and were used for the reconstruction of the pure-dust L2A extinction coefficient.

Aeolus b355nm – co
($\text{Mm}^{-1}\text{Sr}^{-1}$)

Aeolus b355nm – cross
($\text{Mm}^{-1}\text{Sr}^{-1}$)

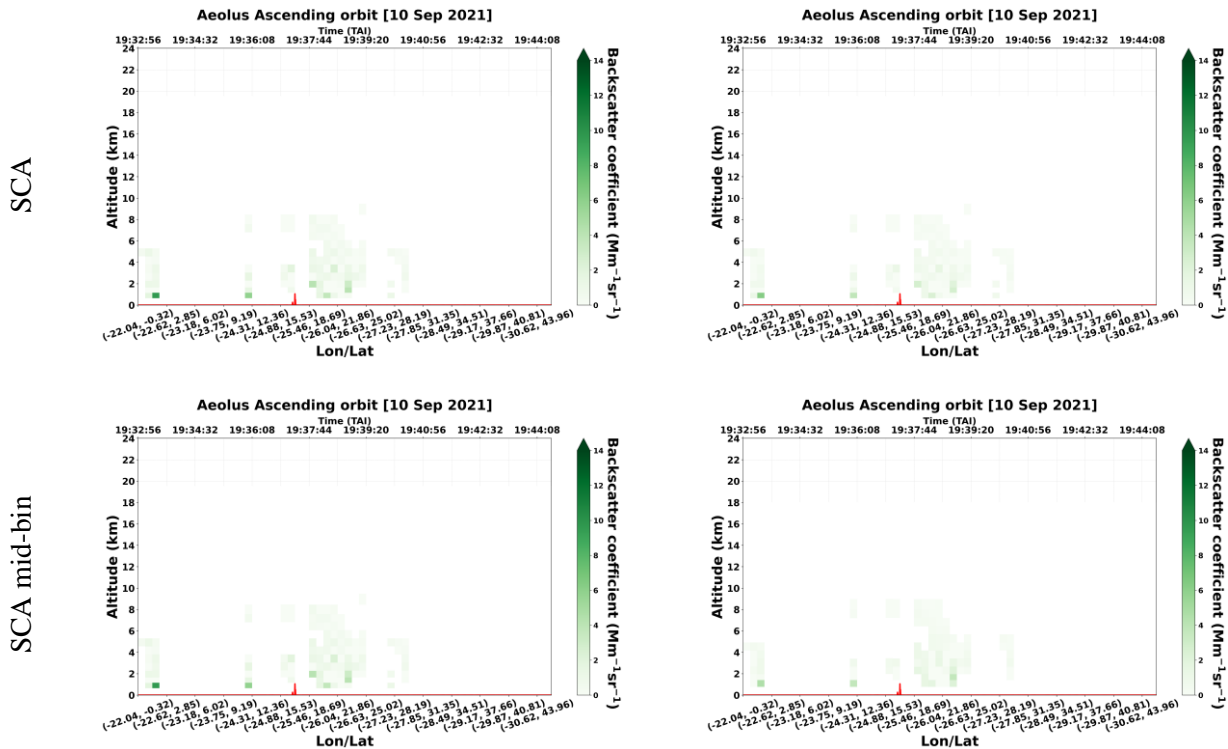


Figure 9: Co-polar and cross polar backscatter profiles along the Aeolus overpass (id 017679) for the SCA (a, b) and SCA mid-bin algorithms (c, d).

3.3.4. L2A+ - ESA-eVe validation.

The present section gives the intercomparison of Aeolus L2A and L2A+ aerosol optical products, in particular the backscatter coefficient at 355 nm retrieved with the SCA, SCA mid-bin and MLE algorithms against ground-based measurements from eVe lidar collected during the ASKOS experiment, under the Joint Aeolus Tropical Atlantic Campaign 2021 (JATAC), on the islands of Cabo Verde. The process was performed considering the raw (unprocessed) Aeolus L2A co-polar backscatter profiles at 355 nm for each of the aforementioned algorithms (SCA, SCA mid-bin, MLE) and the quality-assured (QA) pure-dust total (L2A+) backscatter profiles at 355 nm after the adjustment of the missing cross-polar component. It has to be noted that only the quality-assured (cloud-free) ground-based measurements were used for the comparison process. In the specific example, we present the intercomparison process which serves as a graphic example of the Aeolus performance for the first study case on 10th September 2021 presented in Figure 10.

According to our results, comparing the raw (left panel) and the QA Aeolus retrievals (right panel), it can be noticed that the implementation of the cloud-filtering and dust-typing methodologies for the derivation of the new Aeolus product (L2A+) produces a notable decrease in the amount of available data points since most of bins were rejected from the analysis. This can be noticed at around 6km where the large backscatter coefficients of the raw Aeolus L2A retrievals mostly attributed to cloud presence have been excluded in the QA retrievals. Moreover, looking at the raw Aeolus L2A retrievals, it can also be noticed a surface-related effect in the lowermost bins, retrieving an unreasonably large co-polar backscatter coefficient which was also rejected in the QA retrievals.

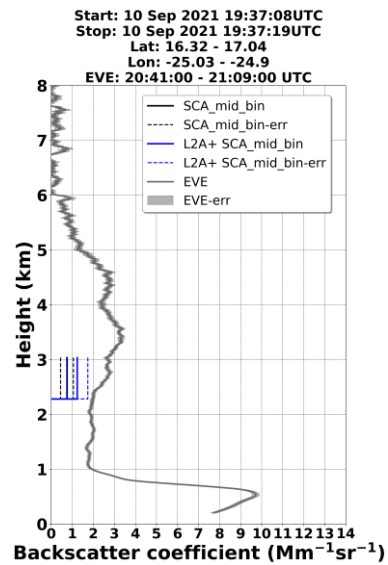
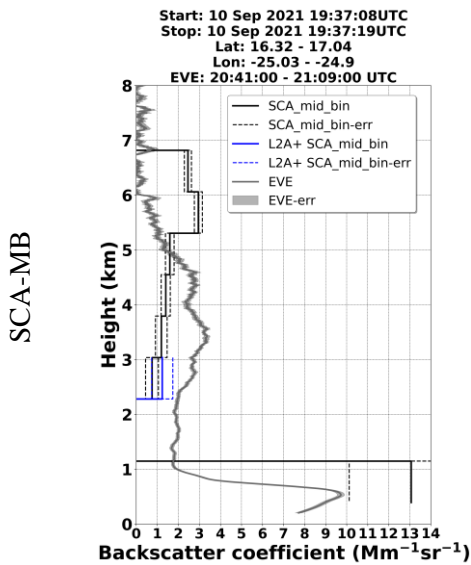
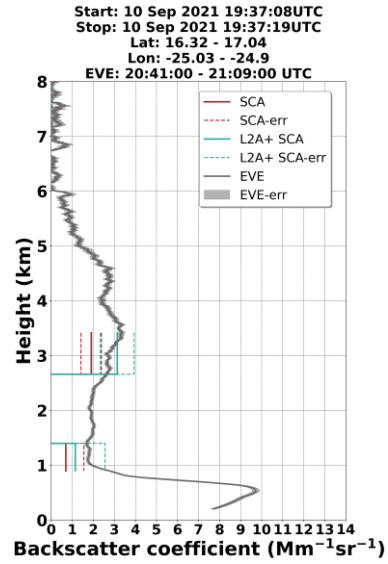
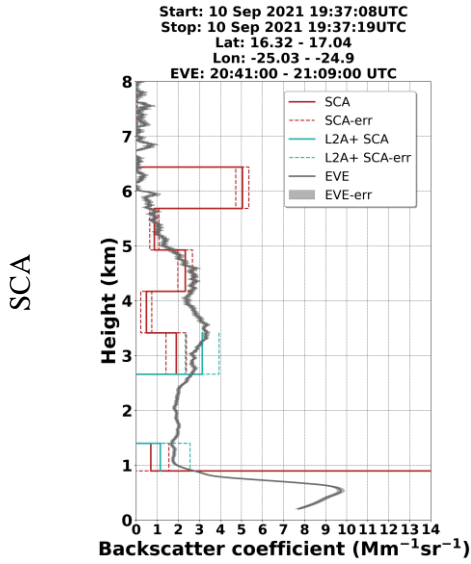
Next, focusing on the pure-dust layers of Aeolus L2A and L2A+ retrievals in Figure 10 (right panel), it can be noticed that after the correction of the backscattered signal, the L2A+ backscatter profiles present a better agreement with ground-based measurements than L2A retrievals. Especially, a fair agreement between the



Aeolus L2A+ backscatter profile for the MLE algorithm and the corresponding ground-based system is pointed out throughout the vertical range of the detected dust layer.

Aeolus b355nm
($\text{Mm}^{-1}\text{sr}^{-1}$)

Aeolus b355nm – AEL-FM & MSG QA
($\text{Mm}^{-1}\text{sr}^{-1}$)



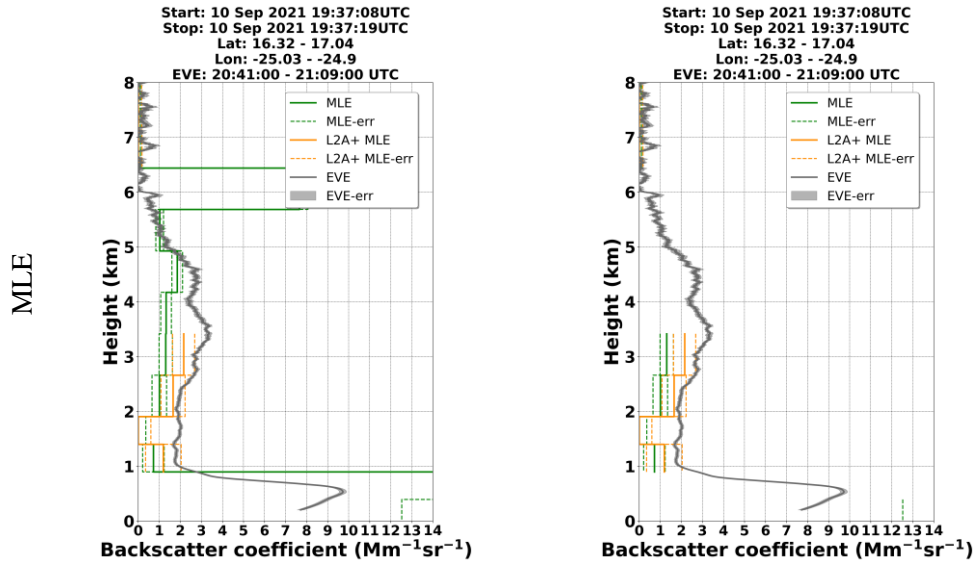


Figure 10: Vertical profiles of the raw Aeolus L2A and QA L2A+ backscatter coefficient at 355 nm retrieved from the SCA, SCA mid-bin and MLE algorithms with the corresponding backscatter profiles at 355 nm acquired by eVe ground-based lidar (left panel), and QA Aeolus L2A and L2A+ backscatter profiles for the SCA, SCA mid-bin and MLE algorithms with the derived backscatter profiles from eVe lidar (right panel).

3.3.5. L2A+ - ESA-PollyXT validation.

The same intercomparison process was also performed between the vertically resolved Aeolus L2A/L2A+ backscatter coefficient at 355 nm for the SCA, SCA mid-bin and MLE algorithms and the corresponding time-nearest backscatter profiles at 532 nm from the Polly^{XT} ground-based lidar operated at Mindelo station, Cabo Verde. The obtained results are presented in Figure 11 for the given study case on 10th September 2021. According to the results, we point out for the pure-dust layers (right panel), that for all the Aeolus L2A retrieval algorithms including the SCA, SCA mid-bin and MLE algorithms, the backscatter coefficient is underestimated throughout the whole vertical range of the detected dust layer. This difference is mostly attributed to the misdetection of the cross-polar component of the backscattered lidar signal when non-spherical mineral particles are recorded. Gkikas et al. (2023) also presented an underestimation that reached up to 33% in the aerosol backscatter coefficient after comparing the PollyXT and Aeolus-like PollyXT backscatter profiles for a study case on 10th July 2019 corroborating our findings. On the other hand, based on our results we can see that this difference is minimized and the satellite presents a satisfactory agreement with PollyXT lidar in the whole available profile when comparing the corrected L2A+ pure-dust total backscatter coefficient with the PollyXT-derived backscatter profile for all the available algorithms.

Aeolus b355nm
(Mm⁻¹sr⁻¹)

Aeolus b355nm – AEL-FM & MSG QA
(Mm⁻¹sr⁻¹)

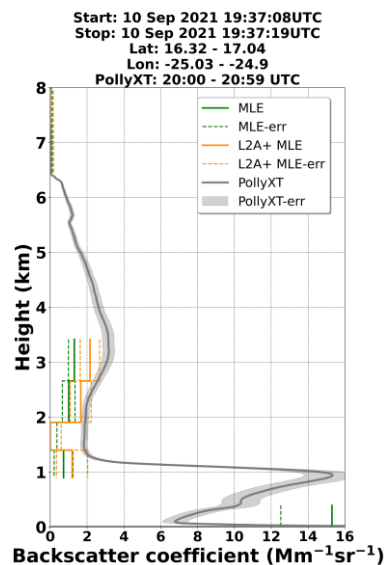
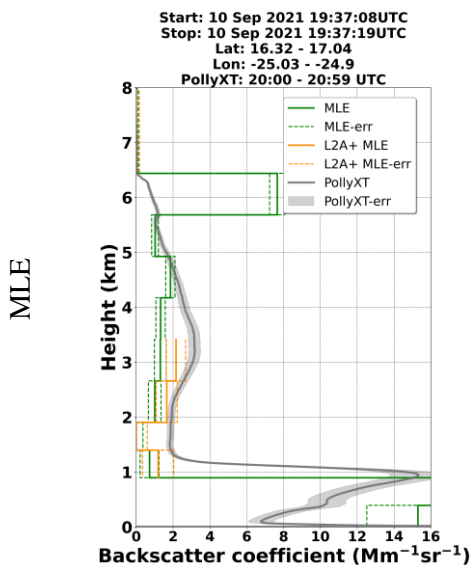
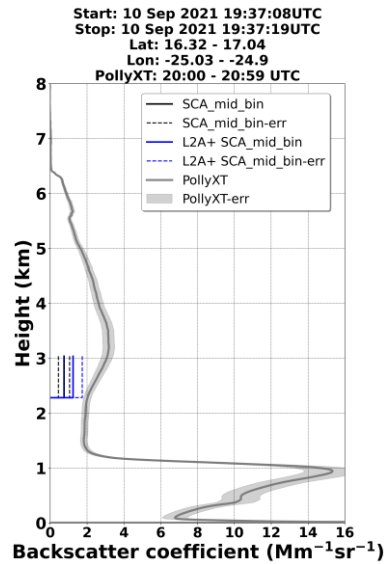
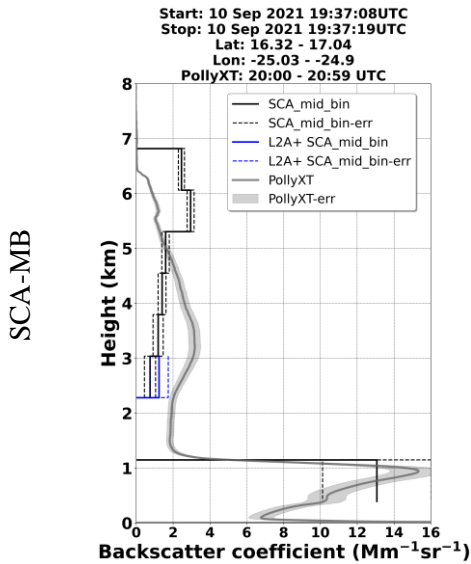
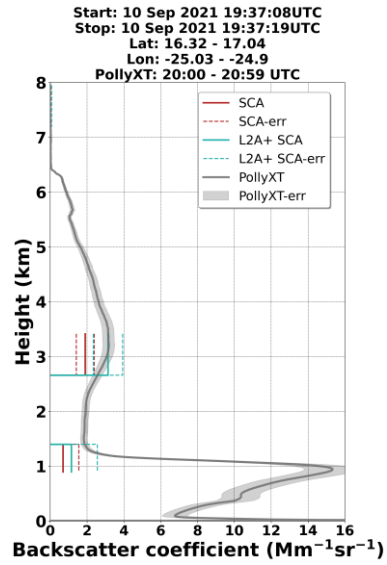
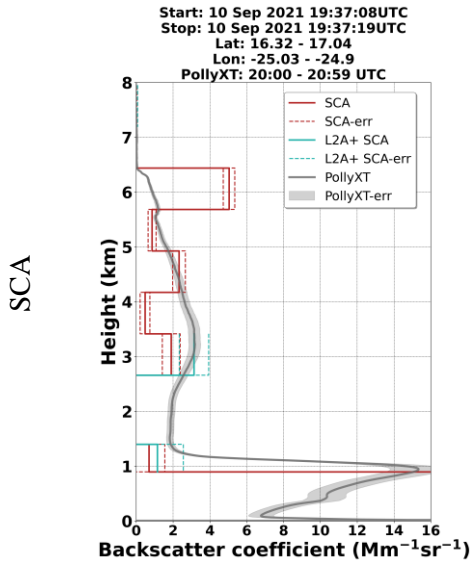




Figure 11: Vertical profiles of the raw Aeolus L2A and QA L2A+ backscatter coefficient at 355 nm retrieved from the SCA, SCA mid-bin and MLE algorithms with the corresponding backscatter profiles at 355 nm acquired by PollyXT ground-based lidar (left panel), and QA Aeolus L2A and L2A+ backscatter profiles for the SCA, SCA mid-bin and MLE algorithms with the derived backscatter profiles from PollyXT lidar (right panel).

3.4. The L2A+ products.

This section provides an overview of the variables included in the L2A+ output files.

Table 5: Detailed description of the groups and variables of the final output L2A+ product.

Group	Subgroup	Variable	Units	Dimensions	Description
GEOLOCATION	DEM_INTERSECTION	measdem	m	1d (measurements)	Altitude relative to the geoid of the intersection of the DEM and the line-of-sight.
		measdomlat	degrees north	1d (measurements)	Latitude of the intersection of the DEM and the line-of-sight.
		measdomlon	degrees east	1d (measurements)	Longitude of the intersection of the DEM and the line-of-sight.
		measdomtime	Date format	1d (measurements)	Measurement centroid time from L1B.
	MIDDLE_BIN_SCALE	alt	m	2d (mb-lays, profs)	Bottom altitude of the middle bin.
		lat	degrees north	2d (mb-lays, profs)	Latitude of the start point of the profile middle bin.
		lon	degrees east	2d (mb-lays, profs)	Longitude of the start point



					of the profile middle bin.
	REGULAR_SCALE	alt	m	2d (lays, profs)	Altitude of the lower edge of the height bin along the line-of-sight.
		lat	degrees north	2d (lays, profs)	Latitude of the lower edge of the height bin along the line-of-sight.
		lon	degrees east	2d (lays, profs)	Longitude of the lower edge of the height bin along the line-of-sight.
RAW DATA	SCA	alpha	10^{-6} m^{-1}	2d (lays, profs)	Particle extinction coefficient of the bin.
		alpha_error	10^{-6} m^{-1}	2d (lays, profs)	Extinction error
		beta	$10^{-6} \text{ sr}^{-1} \text{ m}^{-1}$	2d (lays, profs)	Particle backscatter coefficient of the bin

Figure 12: Raw profiles of L2A SCA extinction coefficient for an indicative Aeolus overpass on 17th of September 2021 (orbit id: 017790).



L2A+

		beta_error	$10^{-6} \text{ sr}^{-1} \text{ m}^{-1}$	2d (lays, profs)	Backscatter error
		<p style="text-align: center;">Aeolus Ascending orbit [17 Sep 2021]</p>			
		lr	sr	2d (lays, profs)	Particle extinction-to-backscatter ratio.
		qcflag	No Units	3d (Qcflags, lays, profs)	QC information about processing (1=data valid, otherwise 0). Bit 1: Extinction, 2: Backscatter, 3: BER, 4: Mie SNR, 5: Rayleigh SNR, 6: Extinction error bar, 7: Backscatter error bar, 8: Cumulative LOD"
		time	Date format	1d (profs)	Start date and time of the SCA profile covered by the present DSR.
	SCA_MID_BIN	alpha	10^{-6} m^{-1}	2d	Particle extinction



			(lays, profs)	coefficient of the middle bin.
alpha_error	10^{-6} m^{-1}	2d	(mb-lays, profs)	Extinction error.
Aeolus Ascending orbit [17 Sep 2021] 				
beta	$10^{-6} \text{ sr}^{-1} \text{ m}^{-1}$	2d	(mb-lays, profs)	Particle backscatter coefficient of the middle bin.
beta_error	$10^{-6} \text{ sr}^{-1} \text{ m}^{-1}$	2d	(mb-lays, profs)	Backscatter error
Aeolus Ascending orbit [17 Sep 2021] 				
lr	sr	2d	(mb-lays, profs)	Particle extinction-to-backscatter



L2A+

				ratio of the middle bin.
		qcflag	No Units (Qcflags, mblays, profs)	QC information about processing.
		time	Date format (profs)	Start date and time of the SCA profile covered by the present DSR.
MLE		alpha	10^{-6} m^{-1} (lays, profs)	Particle extinction coefficient of the bin.
		alpha_error	10^{-6} m^{-1} (lays, profs)	Extinction error
		beta	$10^{-6} \text{ sr}^{-1} \text{ m}^{-1}$ (lays, profs)	Particle backscatter coefficient of the bin
		beta_error	$10^{-6} \text{ sr}^{-1} \text{ m}^{-1}$ (lays, profs)	Backscatter error

Figure 16: Raw profiles of L2A MLE extinction coefficient for an indicative Aeolus overpass on 17th of September 2021 (orbit id: 017790).



	SCA	lr	sr	2d (lays, profs)	Particle extinction-to-backscatter ratio.
CLOUD-FILTERED		alpha	10^{-6} m^{-1}	2d (lays, profs)	Particle extinction coefficient of the bin.
		alpha_error	10^{-6} m^{-1}	2d (lays, profs)	Extinction error
		beta	$10^{-6} \text{ sr}^{-1} \text{ m}^{-1}$	2d (lays, profs)	Particle backscatter coefficient of the bin

Figure 17: Raw profiles of L2A MLE backscatter coefficient for the Aeolus overpass on 17th of September 2021.

Figure 18: Cloud-filtered profiles of L2A SCA extinction coefficient.



		beta_error	$10^{-6} \text{ sr}^{-1} \text{ m}^{-1}$	2d (lays, profs)	Backscatter error
		<p style="text-align: center;">Aeolus Ascending orbit [17 Sep 2021]</p>			
		lr	sr	2d (lays, profs)	Particle extinction-to-backscatter ratio.
	SCA_MID_BIN	alpha	10^{-6} m^{-1}	2d (mb-lays, profs)	Particle extinction coefficient of the middle bin.
		alpha_error	10^{-6} m^{-1}	2d (mb-lays, profs)	Extinction error.
		<p style="text-align: center;">Aeolus Ascending orbit [17 Sep 2021]</p>			
		beta	$10^{-6} \text{ sr}^{-1} \text{ m}^{-1}$	2d (mb-lays, profs)	Particle backscatter

Figure 19: Cloud-filtered profiles of L2A SCA backscatter coefficient.

Figure 20: Cloud-filtered profiles of L2A SCA Mid-Bin extinction coefficient.



				coefficient of the middle bin.
	beta_error	$10^{-6} \text{ sr}^{-1} \text{ m}^{-1}$	2d (mb-lays, profs)	Backscatter error.
	<p style="text-align: center;">Aeolus Ascending orbit [17 Sep 2021]</p>			
	lr	sr	2d (mb-lays, profs)	Particle extinction-to-backscatter ratio of the middle bin.
MLE	alpha	10^{-6} m^{-1}	2d (lays, profs)	Particle extinction coefficient of the bin.
	alpha_error	10^{-6} m^{-1}	2d (lays, profs)	Extinction error
	<p style="text-align: center;">Aeolus Ascending orbit [17 Sep 2021]</p>			
	<p style="text-align: center;"><i>Figure 22: Cloud-filtered profiles of L2A MLE extinction coefficient.</i></p>			



		beta	$10^{-6} \text{ sr}^{-1} \text{ m}^{-1}$	2d (lays, profs)	Particle backscatter coefficient of the bin
		beta_error	$10^{-6} \text{ sr}^{-1} \text{ m}^{-1}$	2d (lays, profs)	Backscatter error
		<p>Figure 23: Cloud-filtered profiles of L2A MLE backscatter coefficient.</p>			
PURE DUST	SCA	alpha	10^{-6} m^{-1}	2d (lays, profs)	Particle extinction coefficient of the bin.
		alpha_error	10^{-6} m^{-1}	2d (lays, profs)	Extinction error.
		<p>Figure 24: Cloud-free dust profiles of L2A SCA extinction coefficient.</p>			
		beta	$10^{-6} \text{ sr}^{-1} \text{ m}^{-1}$	2d (lays, profs)	Particle backscatter



				coefficient of the bin
		beta_error	10 ⁻⁶ sr ⁻¹ m ⁻¹	2d (lays, profs) Backscatter error.
		<p style="text-align: center;">Aeolus Ascending orbit [17 Sep 2021]</p>		
		<p><i>Figure 25: Cloud-free dust profiles of L2A SCA backscatter coefficient.</i></p>		
SCA_MID_BIN	alpha	10 ⁻⁶ m ⁻¹	2d (mb-lays, profs)	Particle extinction coefficient of the middle bin.
	alpha_error	10 ⁻⁶ m ⁻¹	2d (mb-lays, profs)	Extinction error.
	<p style="text-align: center;">Aeolus Ascending orbit [17 Sep 2021]</p>			
	<p><i>Figure 26: Cloud-free dust profiles of L2A SCA Mid-Bin extinction coefficient.</i></p>			
	beta	10 ⁻⁶ sr ⁻¹ m ⁻¹	2d (mb-lays, profs)	Particle backscatter coefficient of the middle bin.



L2A+

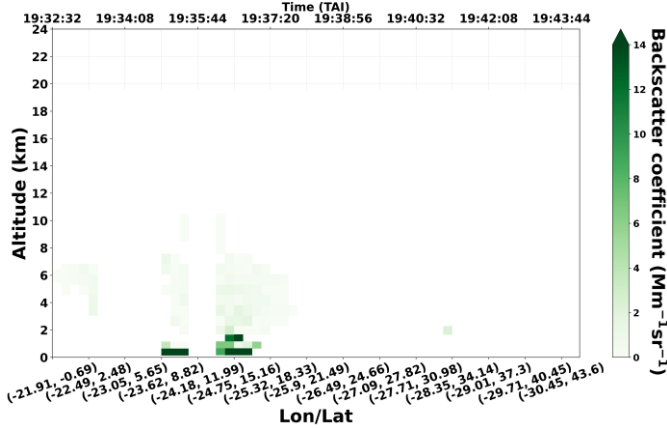
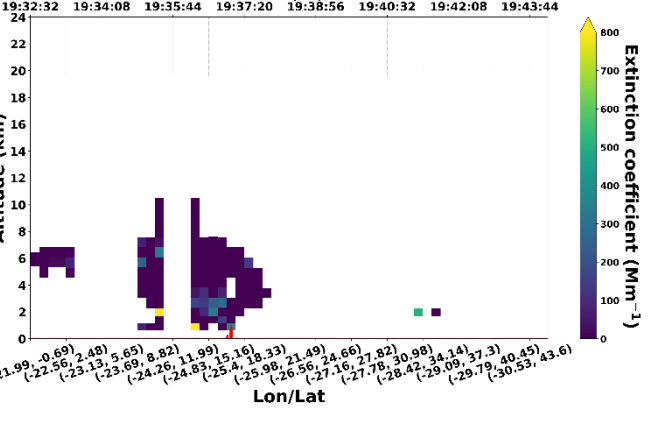
		beta_error	$10^{-6} \text{ sr}^{-1} \text{ m}^{-1}$	2d (mb-lays, profs)	Backscatter error.
		<p style="text-align: center;">Aeolus Ascending orbit [17 Sep 2021]</p>			
	MLE	alpha	10^{-6} m^{-1}	2d (lays, profs)	Particle extinction coefficient of the bin.
		alpha_error	10^{-6} m^{-1}	2d (lays, profs)	Extinction error.
		<p style="text-align: center;">Aeolus Ascending orbit [17 Sep 2021]</p>			
		beta	$10^{-6} \text{ sr}^{-1} \text{ m}^{-1}$	2d (lays, profs)	Particle backscatter coefficient of the bin

Figure 27: Cloud-free dust profiles of L2A SCA Mid-Bin backscatter coefficient.

Figure 28: Cloud-free dust profiles of L2A MLE extinction coefficient.



L2A+

		beta_error $10^{-6} \text{ sr}^{-1} \text{ m}^{-1}$	$10^{-6} \text{ sr}^{-1} \text{ m}^{-1}$	2d (lays, profs)	Backscatter error.
<div style="text-align: center;"> Aeolus Ascending orbit [17 Sep 2021] Time (TAI) 19:32:32 19:34:08 19:35:44 19:37:20 19:38:56 19:40:32 19:42:08 19:43:44  Backscatter coefficient ($\text{Mm}^{-1} \text{sr}^{-1}$) Altitude (km) Lon/Lat (-21.91, -0.69), (-22.49, 2.48), (-23.05, 5.65), (-23.62, 8.82), (-24.18, 11.99), (-24.75, 15.16), (-25.32, 18.33), (-25.9, 21.49), (-26.49, 24.66), (-27.09, 27.82), (-27.71, 30.98), (-28.35, 34.14), (-29.01, 37.3), (-29.71, 40.45), (-30.45, 43.6) </div> <p>Figure 29: Cloud-free dust profiles of L2A MLE backscatter coefficient.</p>					
L2APLUS	SCA	beta_co $10^{-6} \text{ sr}^{-1} \text{ m}^{-1}$	$10^{-6} \text{ sr}^{-1} \text{ m}^{-1}$	2d (lays, profs)	Co-component of backscatter coefficient.
<div style="text-align: center;"> Aeolus Ascending orbit [17 Sep 2021] Time (TAI) 19:32:32 19:34:08 19:35:44 19:37:20 19:38:56 19:40:32 19:42:08 19:43:44  Extinction coefficient (Mm^{-1}) Altitude (km) Lon/Lat (-21.99, -0.69), (-22.56, 2.48), (-23.13, 5.65), (-23.69, 8.82), (-24.26, 11.99), (-24.83, 15.16), (-25.4, 18.33), (-25.98, 21.49), (-26.56, 24.66), (-27.16, 27.82), (-27.78, 30.98), (-28.42, 34.14), (-29.09, 37.3), (-29.79, 40.45), (-30.53, 43.6) </div> <p>Figure 30: Provides the vertical profiles of the co-component of backscatter coefficient along the Aeolus overpass.</p>					
		beta_cross $10^{-6} \text{ sr}^{-1} \text{ m}^{-1}$	$10^{-6} \text{ sr}^{-1} \text{ m}^{-1}$	2d (lays, profs)	Cross-component of backscatter coefficient.

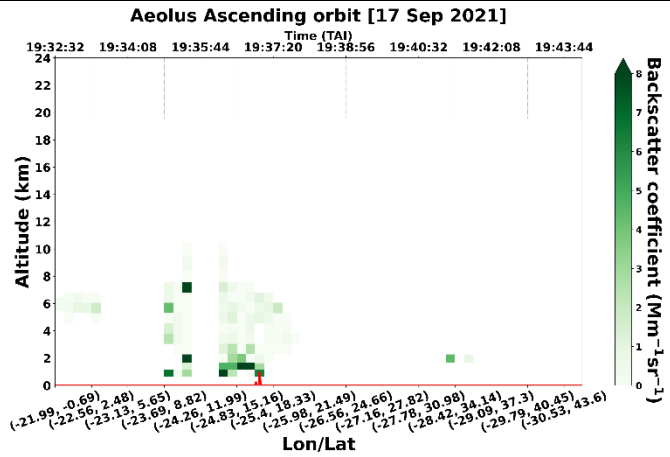


Figure 31: Profiles of the SCA Cross-component backscatter coefficient along the Aeolus overpass (id:017790).

beta_total	$10^{-6} \text{ sr}^{-1} \text{ m}^{-1}$	2d (lays, profs)	Total backscatter coefficient.
------------	--	---------------------	--------------------------------

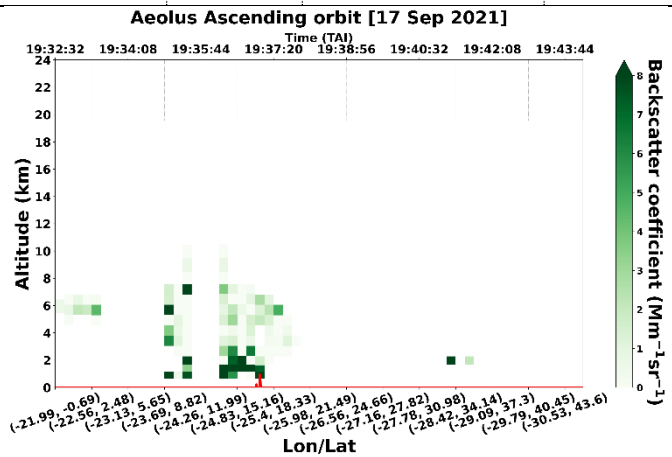


Figure 32: Profiles of the total (co + cross components) SCA backscatter coefficient.

alpha_plus_355	10^{-6} m^{-1}	2d (lays, profs)	L2A+ extinction coefficient at 355nm.
----------------	--------------------------	---------------------	---------------------------------------

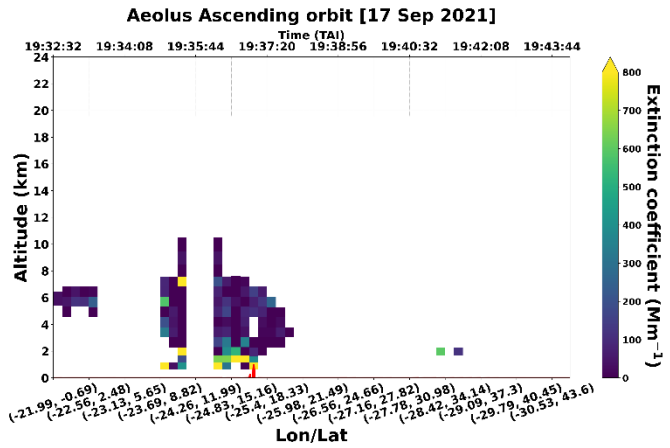


Figure 33: Profiles of the reconstructed L2A+ SCA extinction coefficient at 355nm.

alpha_plus_532	10^{-6} m^{-1}	2d (lays, profs)	L2A+ extinction coefficient at 532nm.
----------------	--------------------------	---------------------	--

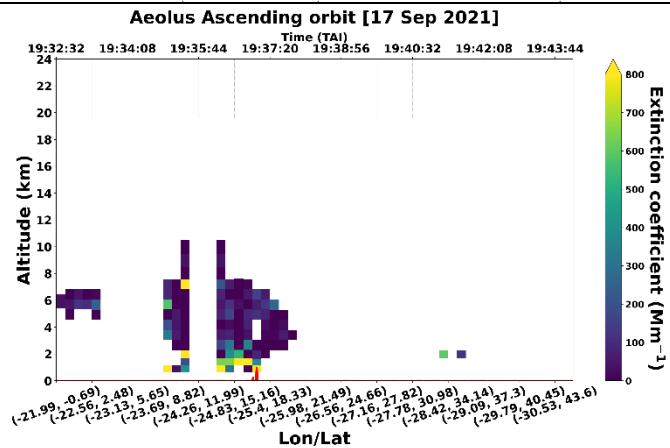


Figure 34: Profiles of the reconstructed L2A+ SCA extinction coefficient at 532nm.

dust_concentr.	$\mu\text{g}/\text{m}^3$	2d (lays, profs)	Dust mass concentration.
----------------	--------------------------	---------------------	-----------------------------

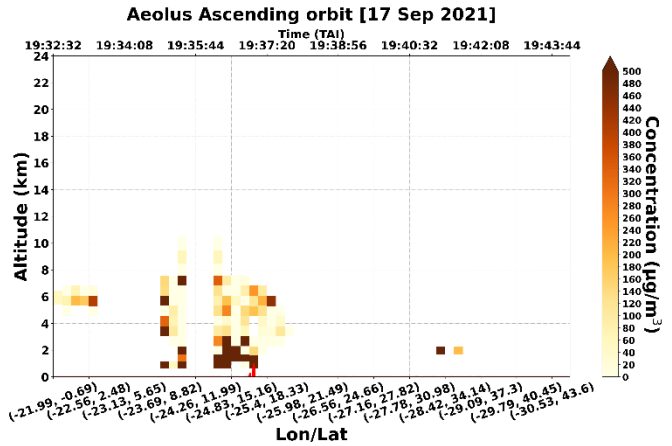


Figure 35: Profiles of the L2A+ dust mass concentration along the Aeolus overpass (id:017790).

SCA_MID_BIN

beta_co	$10^{-6} \text{ sr}^{-1} \text{ m}^{-1}$	2d (mb-lays, profs)	Co-component of backscatter coefficient at 355nm.
---------	--	------------------------	---

See Figure 13 which gives vertical profiles of the co-component of backscatter coefficient at Mid-Bin scale along the Aeolus overpass.

beta_cross	$10^{-6} \text{ sr}^{-1} \text{ m}^{-1}$	2d (mb-lays, profs)	Cross-component of backscatter coefficient at 355 nm.
------------	--	------------------------	---

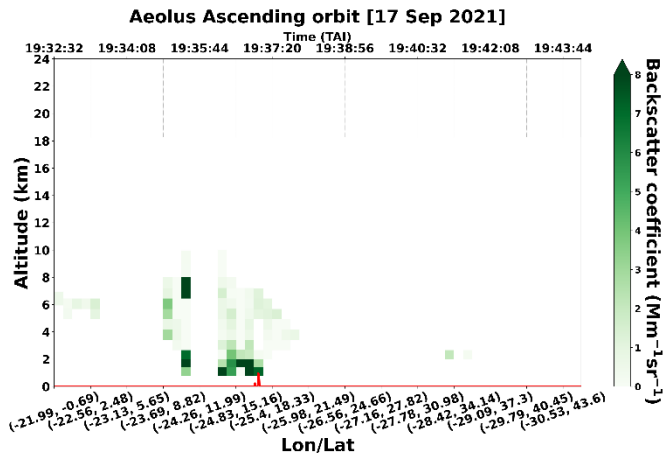


Figure 36: Profiles of the SCA Mid-Bin Cross-component backscatter coefficient along the Aeolus overpass (id:017790).

beta_total	$10^{-6} \text{ sr}^{-1} \text{ m}^{-1}$	2d (mb-lays, profs)	Total backscatter coefficient at 355nm.
------------	--	------------------------	---

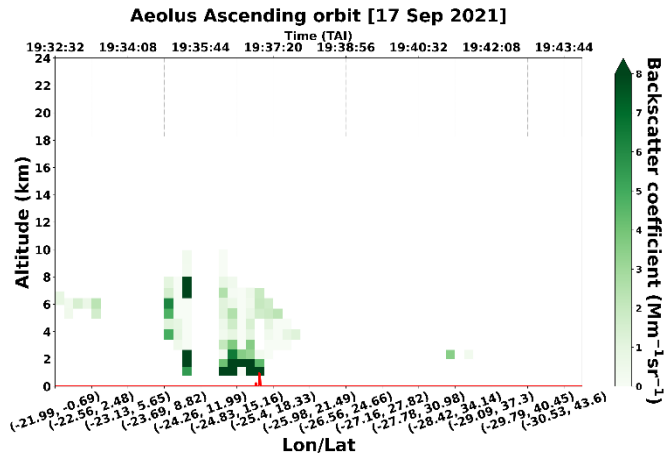


Figure 37: Profiles of the total (co + cross components) SCA Mid-Bin backscatter coefficient.

alpha_plus_355	10^{-6} m^{-1}	2d (mb-lays, profs)	L2A+ extinction coefficient at 355nm.
----------------	--------------------------	------------------------	--

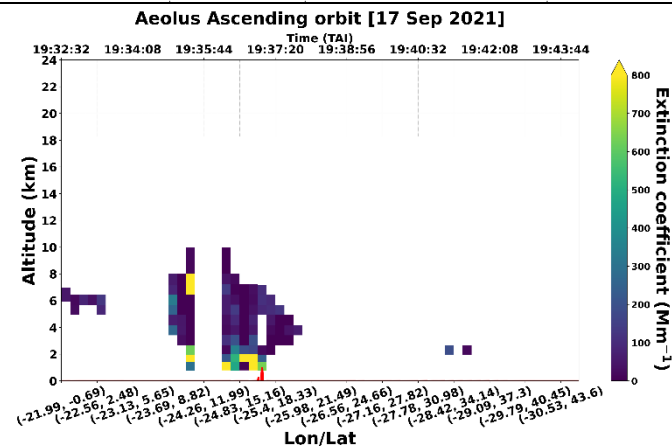


Figure 38. Profiles of the reconstructed L2A+ SCA Mid-Bin extinction coefficient at 355nm.

alpha_plus_532	10^{-6} m^{-1}	2d (mb-lays, profs)	L2A+ extinction coefficient at 532nm.
----------------	--------------------------	------------------------	--

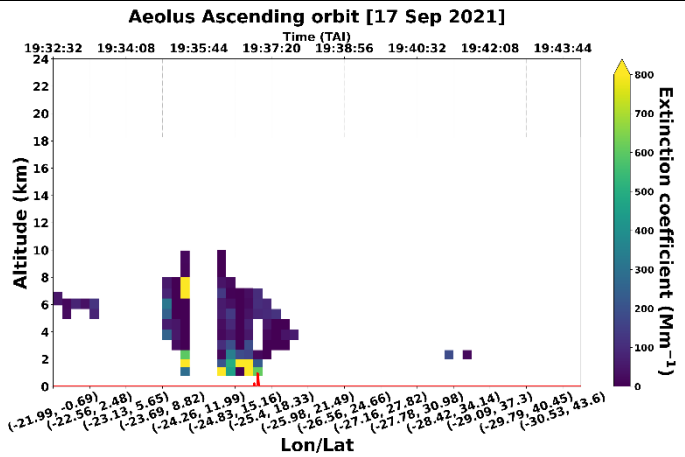


Figure 39. Profiles of the reconstructed L2A+ SCA Mid-Bin extinction coefficient at 532nm.

dust_concentr.	$\mu\text{g}/\text{m}^3$	2d	Dust mass concentration.
		(mb-lays, profs)	

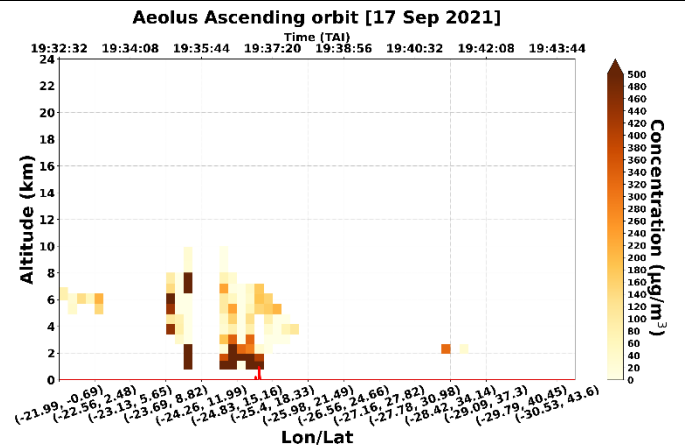


Figure 40: Profiles of the L2A+ dust mass concentration at Mid-Bin scale along the Aeolus overpass (id:017790).

MLE	beta_co	$10^{-6} \text{ sr}^{-1} \text{ m}^{-1}$	2d	Co-component of backscatter coefficient.
			(lays, profs)	

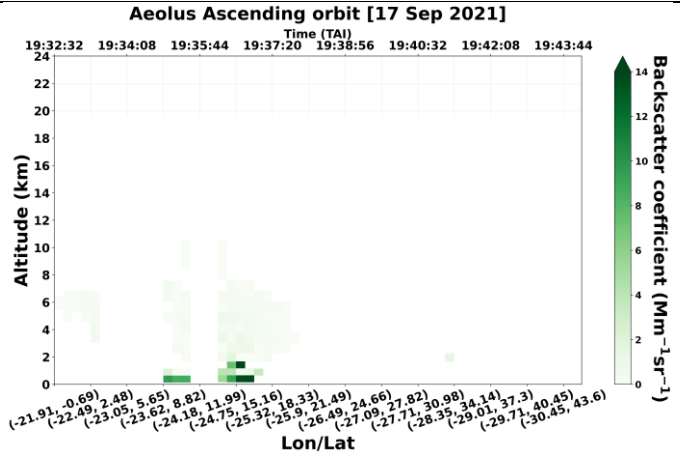


Figure 41: Vertical profiles of the MLE co-component of backscatter coefficient along the Aeolus overpass.

beta_cross	$10^{-6} \text{ sr}^{-1} \text{ m}^{-1}$	2d (lays, profs)	Cross-component of backscatter coefficient.
------------	--	---------------------	---

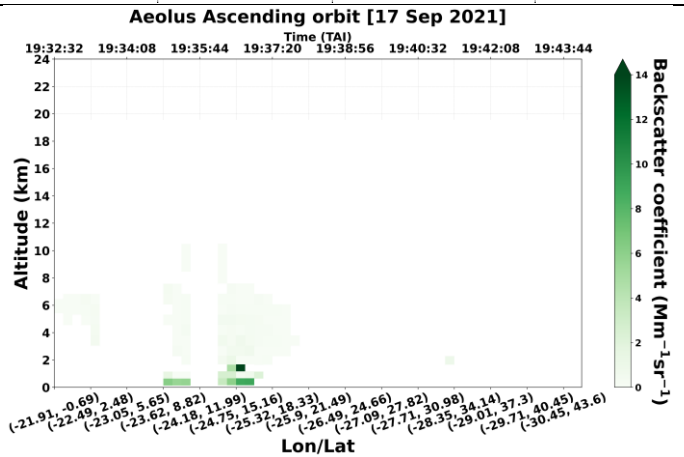


Figure 42: Profiles of the MLE Cross-component backscatter coefficient along the Aeolus overpass (id:017790).

beta_total	$10^{-6} \text{ sr}^{-1} \text{ m}^{-1}$	2d (lays, profs)	Total backscatter coefficient.
------------	--	---------------------	--------------------------------

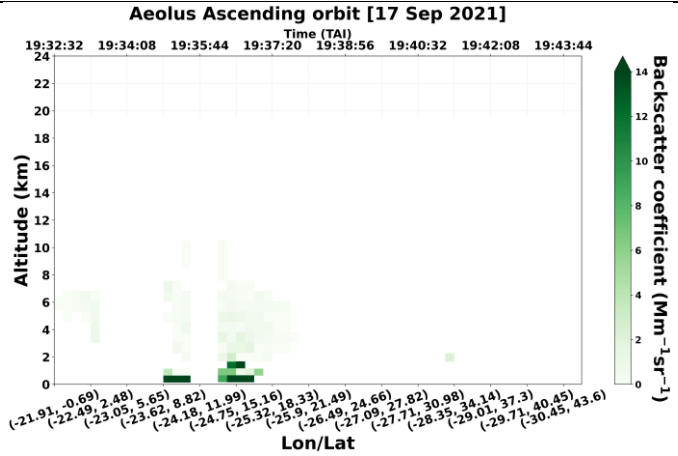


Figure 43: Profiles of the total (co + cross components) MLE backscatter coefficient.

alpha_plus_355	10^{-6} m^{-1}	2d (lays, profs)	L2A+ extinction coefficient at 355nm.
----------------	--------------------------	---------------------	---------------------------------------

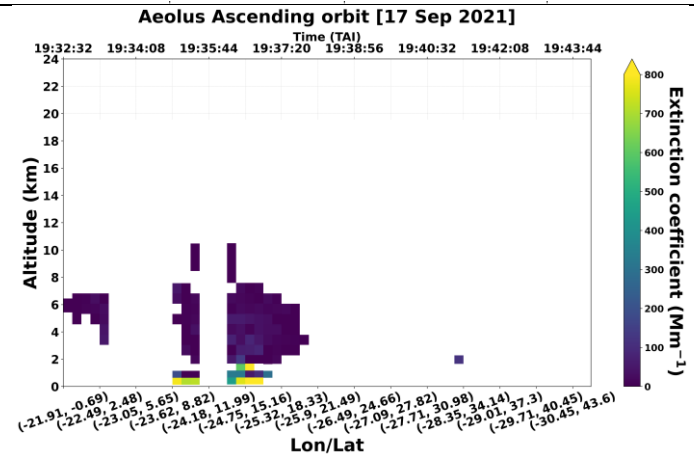


Figure 44. Profiles of the reconstructed L2A+ MLE extinction coefficient at 355nm.

alpha_plus_532	10^{-6} m^{-1}	2d (lays, profs)	L2A+ extinction coefficient at 532nm.
----------------	--------------------------	---------------------	---------------------------------------

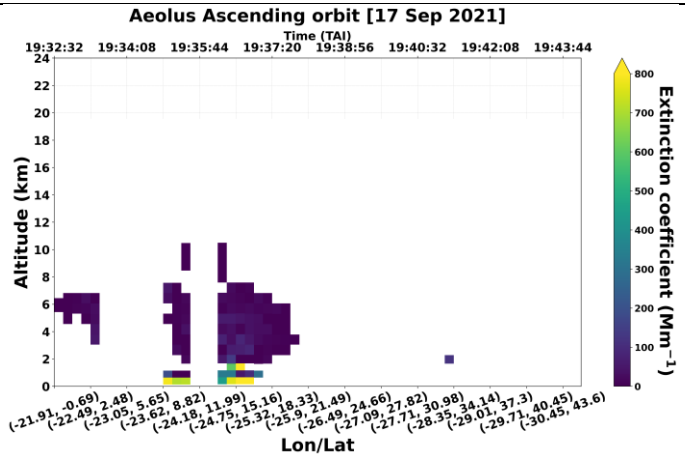


Figure 45. Profiles of the reconstructed L2A+ MLE extinction coefficient at 532nm.

dust_concentr.	$\mu\text{g}/\text{m}^3$	2d	Dust mass concentration.
		(lays, profs)	

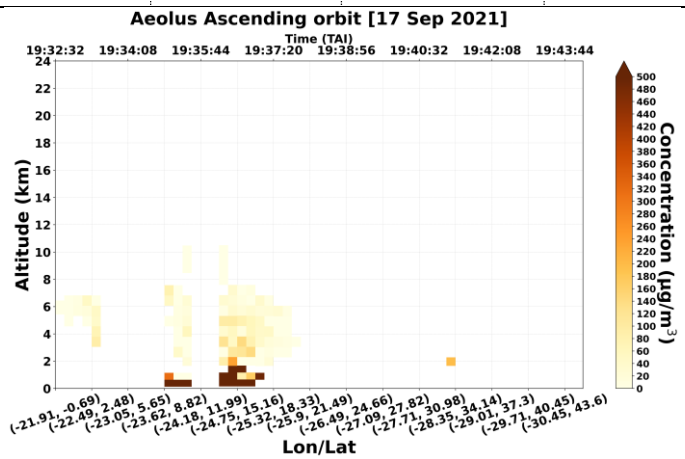


Figure 46. Profiles of the L2A+ MLE dust mass concentration along the Aeolus overpass (id:017790).



L2A+

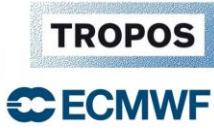
Ref: Ref: ESA AO/1-11041/22/I-NS

DI05: Output Data Product (OP) - V2

Page: 48

Name	Long Name	Type
AE_OPER_ALD_U_N_2A_20210910T181932020_00...	AE_OPER_ALD_U_N_2A_20210910T181932020_008508008...	Local File
▼ CLOUD_FILTERED	CLOUD_FILTERED	—
▶ MLE	MLE	—
▶ SCA	SCA	—
▶ SCA_MID_BIN	SCA_MID_BIN	—
▼ GEOLOCATION	GEOLOCATION	—
▶ DEM_INTERSECTION	DEM_INTERSECTION	—
▶ MIDDLE_BIN_SCALE	MIDDLE_BIN_SCALE	—
▶ REGULAR_SCALE	REGULAR_SCALE	—
▼ L2APLUS	L2APLUS	—
▼ MLE	MLE	—
alpha_plus_355	L2A+ extinction coefficient at 355nm	2D
alpha_plus_532	L2A+ extinction coefficient at 532nm	2D
beta_co	Co-component of backscatter coefficient	2D
beta_cross	Cross-component of backscatter coefficient	2D
beta_total	Total backscatter coefficient	2D
dust_concentration	Dust mass concentration	2D
▶ SCA	SCA	—
▶ SCA_MID_BIN	SCA_MID_BIN	—
▼ PURE_DUST	PURE_DUST	—
▶ MLE	MLE	—
▶ SCA	SCA	—
▶ SCA_MID_BIN	SCA_MID_BIN	—
▼ RAW_DATA	RAW_DATA	—
▶ MLE	MLE	—
▶ SCA	SCA	—
▶ SCA_MID_BIN	SCA_MID_BIN	—

Figure 47: Indicative file output of the L2A/L2A+ optical properties.



L2A+

3.5. Access Credential.

Access to the ESA-L2A+ products are provided according to the following access credentials:

Table 6: ESA-L2A+ WP3000 access credentials.

L2A+ OPs	
Protocol:	SFTP (Port 22)
Username:	l2aplus_wp2000
Password:	eYst5kuxngzn
Host:	react.space.noa.gr

3.6. Contact Person.

Contact:

Users can contact with Konstantinos Rizos (k.rizos@noa.gr) for any further details and clarifications regarding the L2A+ dataset.



Acronyms and Abbreviations

L2A	Aeolus Level 2A product
L2A+	Improved Aeolus Level 2A product
SCA	Standard Correct Algorithm
SCA MID BIN	Standard Correct Algorithm at the Middle-Bin vertical scale

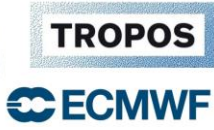
List of Figures

Figure	Description
01	ESA-L2A+ WP2000, WP3000, and WP4000 input and outputs relevant to DI05
02	Indicative file output of Unique feature mask over Mindelo.
03	Indicative file output of PollyXT optical properties.
04	a) Aeolus ascending orbit (id: 017679) over the L2A+ RoI on 10th September 2021 and b) the time-closest spatial distribution of clouds derived from the binary cloud-mask product of MSG-SEVIRI CLAAS-3 dataset
05	a) AEL-FM feature mask product along the Aeolus orbit (id: 017679) on 10th September 2021 and the transformed feature mask product on the Aeolus vertical and horizontal resolution for the b) regular (24 bins) and c) middle-bin scale (23 bins).
06	Vertical profiles of CAMS dust mass concentration and dust-to-total aerosol mass concentration ratio along the Aeolus orbit (id: 017679) provided in the regular (a, b) and middle-bin (c, d) vertical scales on the 10th of September 2021.
07	(a) CALIPSO total backscatter coefficient at 532 nm. (b) CALIPSO particulate depolarization ratio at 532 nm (c) CALIPSO QA pure-aerosol total backscatter coefficient at 532 nm (d) CALIPSO QA pure-dust backscatter coefficient at 532 nm.
08	Raw Aeolus L2A backscatter profiles at 355 nm along the Aeolus orbit (id 017679) retrieved from the SCA, SCA mid-bin and MLE algorithms (left panel) and the corresponding QA pure-aerosol backscatter profiles at 355 nm for the SCA, SCA mid-bin and MLE algorithms (right panel).
09	Co-polar and cross polar backscatter profiles along the Aeolus overpass (id 017679) for the SCA (a, b) and SCA mid-bin algorithms (c, d).
10	Vertical profiles of the raw Aeolus L2A and QA L2A+ backscatter coefficient at 355 nm retrieved from the SCA, SCA mid-bin and MLE algorithms with the corresponding backscatter profiles at 355 nm acquired by eVe ground-based lidar (left panel), and QA Aeolus L2A and L2A+ backscatter profiles for the SCA, SCA mid-bin and MLE algorithms with the derived backscatter profiles from eVe lidar (right panel).
11	Vertical profiles of the raw Aeolus L2A and QA L2A+ backscatter coefficient at 355 nm retrieved from the SCA, SCA mid-bin and MLE algorithms with the corresponding backscatter profiles at 355 nm acquired by PollyXT ground-based lidar (left panel), and QA Aeolus L2A and L2A+ backscatter profiles for the SCA, SCA mid-bin and MLE algorithms with the derived backscatter profiles from PollyXT lidar (right panel).
12	Raw profiles of L2A SCA extinction coefficient for an indicative Aeolus overpass on 17th of September 2021 (orbit id: 017790).
13	Raw profiles of L2A SCA backscatter coefficient for the Aeolus overpass on 17th of September 2021.



L2A+

14	Raw profiles of L2A SCA Mid-Bin extinction coefficient for the Aeolus overpass on 17th of September 2021.
15	Raw profiles of L2A SCA Mid-Bin backscatter coefficient for the Aeolus overpass on 17th of September 2021.
16	Raw profiles of L2A MLE extinction coefficient for an indicative Aeolus overpass on 17th of September 2021 (orbit id: 017790).
17	Raw profiles of L2A MLE backscatter coefficient for the Aeolus overpass on 17th of September 2021.
18	Cloud-filtered profiles of L2A SCA extinction coefficient.
19	Cloud-filtered profiles of L2A SCA backscatter coefficient.
20	Cloud-filtered profiles of L2A SCA Mid-Bin extinction coefficient.
21	Cloud-filtered profiles of L2A SCA Mid-Bin backscatter coefficient.
22	<i>Cloud-filtered profiles of L2A MLE extinction coefficient.</i>
23	Cloud-filtered profiles of L2A MLE backscatter coefficient.
24	Cloud-free dust profiles of L2A SCA extinction coefficient.
25	Cloud-free dust profiles of L2A SCA backscatter coefficient.
26	Cloud-free dust profiles of L2A SCA Mid-Bin extinction coefficient.
27	Cloud-free dust profiles of L2A SCA Mid-Bin backscatter coefficient.
28	Cloud-free dust profiles of L2A MLE extinction coefficient.
29	Cloud-free dust profiles of L2A MLE backscatter coefficient.
30	Provides the vertical profiles of the co-component of backscatter coefficient along the Aeolus overpass.
31	Profiles of the SCA Cross-component backscatter coefficient along the Aeolus overpass (id:017790).
32	Profiles of the total (co + cross components) SCA backscatter coefficient.
33	Profiles of the reconstructed L2A+ SCA extinction coefficient at 355nm.
34	Profiles of the reconstructed L2A+ SCA extinction coefficient at 532nm.
35	Profiles of the L2A+ dust mass concentration along the Aeolus overpass (id:017790).
36	Profiles of the SCA Mid-Bin Cross-component backscatter coefficient along the Aeolus overpass (id:017790).
37	Profiles of the total (co + cross components) SCA Mid-Bin backscatter coefficient.
38	Profiles of the reconstructed L2A+ SCA Mid-Bin extinction coefficient at 355nm.
39	Profiles of the reconstructed L2A+ SCA Mid-Bin extinction coefficient at 532nm.
40	Profiles of the L2A+ dust mass concentration at Mid-Bin scale along the Aeolus overpass (id:017790).
41	Vertical profiles of the MLE co-component of backscatter coefficient along the Aeolus overpass.
42	Profiles of the MLE Cross-component backscatter coefficient along the Aeolus overpass (id:017790).
43	Profiles of the total (co + cross components) MLE backscatter coefficient.
44	Profiles of the reconstructed L2A+ MLE extinction coefficient at 355nm.
45	Profiles of the reconstructed L2A+ MLE extinction coefficient at 532nm.
46	Profiles of the L2A+ MLE dust mass concentration along the Aeolus overpass (id:017790).
47	Indicative file output of the L2A/L2A+ optical properties.



L2A+

Ref: *Ref: ESA AO/1-11041/22/I-NS*
DI05: Output Data Product (OP) - V2
Page: 52

List of Tables

Table	Description
01	Provides the vertical profiles of the co-component of backscatter coefficient along the Aeolus overpass.
02	Detailed description of the variables within the PollyXT profile product.
03	ESA L2A+ WP2000 access credentials.
04	L2A+ filename descriptor.
05	Detailed description of the groups and variables of the final output L2A+ product.
06	ESA-L2A+ WP3000 access credentials.



L2A+

Ref: *Ref: ESA AO/1-11041/22/I-NS*

DI05: Output Data Product (OP) - V2

Page: 53

[End of ESA-L2A+ DI05 – OP – V2.0]